# Materials and Nanotechnology

# introduction

The focus of the **Materials and Nanotechnology Program** is technology development related to processing, analysis, testing and characterization of materials in general. These are achieved through execution of R&D projects in engineering and materials science, cooperative projects with private and public sector companies, universities and other research institutes. Besides technology development, this Program also fosters training and human resource development in association with the University of São Paulo and many industrial sectors. This Program is divided into sub-programs in broad areas such as ceramic, composite and metallic materials as well as characterization of physical and chemical properties of materials. The sub-programs are further divided into general topics and within each topic, R&D projects. A brief description of progress in each topic during the last three years follows.

### Biomedical metals and alloys prepared by powder metallurgy

Biomaterials for use in implants must be biocompatible, bio-functional and resistant to corrosion. Utilization of titanium and its alloys is continuously increasing due to their higher strength to weight ratio, superior biocompatibility and corrosion resistance, good mechanical properties and low elastic modulus compared to other metallic biomaterials such as stainless steels and Co-Cr alloys. Use of materials with low elastic modulus close to that of bone is essential to reduce stress effects, which can cause loosening of the implant. Nevertheless, higher reactivity of this metal in the liquid phase makes manufacture of Ti alloy implants difficult and expensive to produce using the conventional melting and casting technique. Hence an alternate route to reduce processing temperature and cost is to use the powder metallurgy (PM) technique. This procedure enables the manufacture of implants with porous surfaces that improve osseointegration, which favors transport of body fluids. The micrograph in Figure 1 shows that it is possible to obtain samples with controlled porosity after uniaxial compaction at 400 MPa and vacuum sintering at 1150°C. Potentiodynamic polarization measurements indicated high resistance to corrosion and biocompatibility in Hanks' solution.

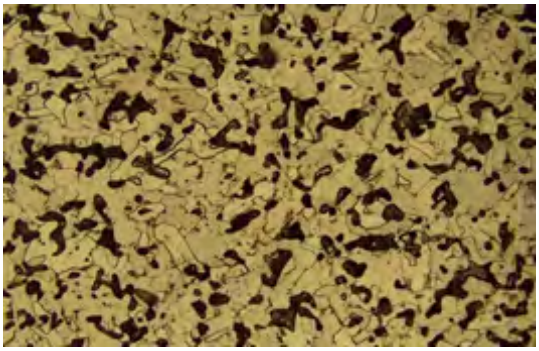

Figure 1. Optical micrograph of a sintered Ti sample produced by powder metallurgy.

Many low-modulus titanium alloys for biomedical implants contain large quantities of alloying elements with melting points higher than that of Ti, making PM processing advantageous, as it results in producing homogeneous microstructures at temperatures below the melting point. The ternary Ti-13Nb-13Zr alloy has only biocompatible elements and has a lower elastic modulus than the Co-Cr alloy, stainless steel and Ti6Al4V alloy, as well as higher corrosion resistance. The Ti-13Nb-13Zr alloy was prepared using the PM technique in which elemental hydride powders were blended followed by high energy planetary ball milling, cold isostatic pressing and sintering under high vacuum. Figure 2 shows a SEM image of Ti13Nb13Zr alloy produced by powder metallurgy using milling speed of 200 rpm during 180 min, and sintering at 1150°C for 10h.

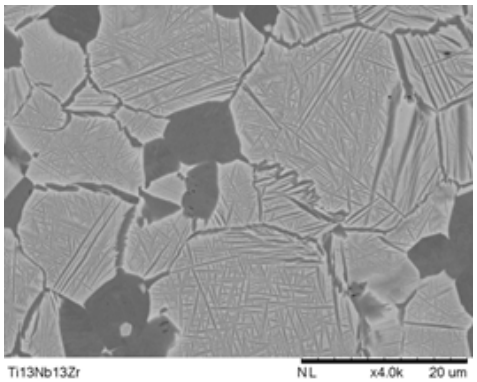


Figure 2. SEM image of Ti13Nb13Zr alloy produced by PM and sintered at 1150°C for 10h.

Studies carried out to produce porous metallic biomaterials with commercially pure titanium (cpTi) and Ti-13Nb-13Zr using the PM route and with additives such as gelatin, starches, albumin, either as space-holder or as a suspension, were done with the objective of resolving problems related to interaction between material and bone in the organism. The molecular profile of tissue response to a titanium implant with a structurally graded interface was also studied. The microarchitecture of these porous materials should mimic bone structure in the area where it is being used. This feature depends on the processing technique as well as the type of natural polymer that is used. Biological characterization, *in vitro* and *in vivo* helps reveal if the use of the implants in humans is promising. Therefore the reaction of living organisms to these materials needs to be reviewed. After verification of non-toxicity, the materials are implanted in rabbits to evaluate the more complex process of osseointegration of the porous material. Pore size obtained by this technique allowed proper nourishment for cell survival, proving that pores and channels formed a highly interconnected network aiding osseointegration and osteoconduction of the porous alloy. Osseointegration inside porous implants have been poorly evaluated in many studies. Therefore an improved method of characterization was developed by the group, with the use of lectinhistochemistry, SEM and SEM-EDS (Figure 3).

Besides obtaining porous implants, Ti:Nb:Zr alloys with varying composition and Young's modulus, compatible with the elastic modulus of human bone, 10 - 30 GPa, were also obtained using the PM technique. The Ti27Nb13Zr alloy, classified as α + β, had elastic modulus of ~ 76 GPa and hardness of ~ 610 HV. Figure 4 shows the micrograph of a sample sintered at 1300°C for 3 h.

Modifications to the metal surface for suitable osseointegration are being investigated. It is desirable to provide a bone-bonding ability to Ti metal and its alloys. This ability can be achieved by surface modification using chemical treatments. The chemical treatment methods include acid-etching, oxidation with hydrogen peroxide, alkali-heating or acid-alkali procedure, etc. After chemical and thermal treatments, titanium and its alloys can be made bioactive by using a technique to produce biomimetic coatings. This method consists of nucleation and crystal growth of apatites similar to bone on titanium and its alloys. Coatings are carried out with a simulated body fluid (SBF), the ion concentration, temperature and pH of which are adjusted to almost match that of human blood plasma. Biomimetic synthesis of calcium phosphate layers is a promising coating method to produce implants with bioactive surfaces because the layer has a Ca/P ratio similar to biological bone apatite and integrates with the titanium substrate with a graded structure without a distinct interface. The bioactive titanium and its alloys create a favorable template for osteoblast migration, differentiation and bone formation.

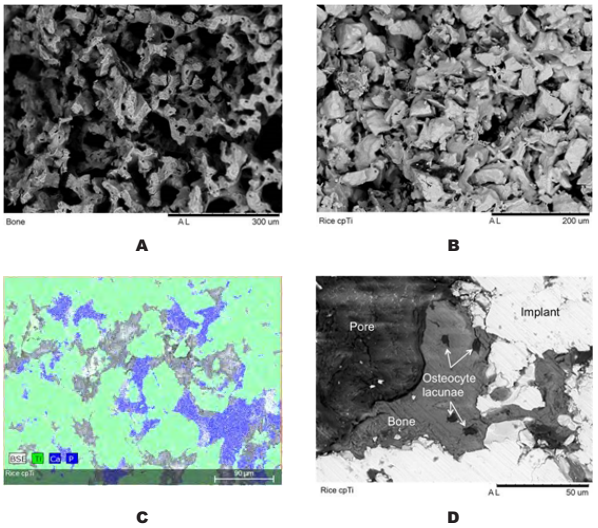


Figure 3. A) Scanning electron micrograph (SEM) of rabbit proximal tibia trabecular bone, region with heterogeneous pore size distribution and irregular pore shape; B) scanning electron micrograph of fractured sample to which rice starch was added; C) SEM-EDS analysis of implant prepared with rice starch, composite image highlighting Ti (green) and Ca/P (blue); D) SEM of implant prepared with rice starch, undecalcified histological slide revealing bone-implant interface and pores; osteocyte lacunae are indicated with arrows.

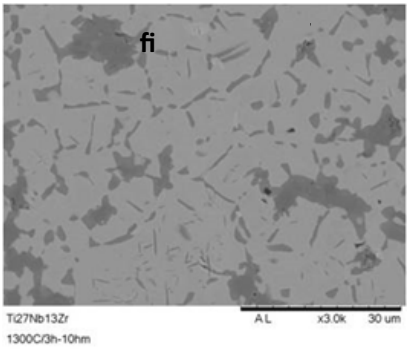


Figure 4. SEM of Ti-27Nb-13Zr treated 1300°C for 3 h.

Rolled titanium and samples of Ti and Ti-13Nb-13Zr alloy obtained by powder metallurgy were compared for their apatite-forming ability in SBF after they were given different pre-treatments for 1, 3, 6, 9, 15 and 21 days. The following pretreatments were studied: alkali; alkali and heat; acid and alkali; alkali-$CaCl_2$-heat and hot water. Apatite formation was observed in all groups; however, the apatite-coating was more effective in samples obtained by powder metallurgy (Figure 5). The Ti27Nb13Zr alloy was immersed in SBF solution for periods of 3, 7, 11 and 15 days and exhibited calcium phosphate layers from the third day of immersion in SBF as shown in Figure 6.

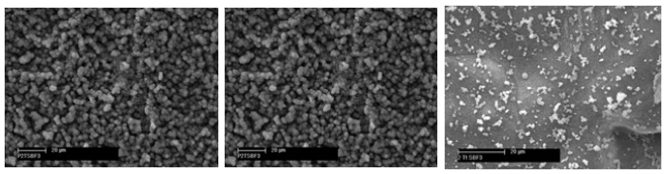

Figure 5. SEM micrographs of surfaces of P/M (a-Ti; b-Ti-13Nb-13Zr) and rolled (c-Ti) given acid and alkali-treatment and soaked in SBF for 3 days.

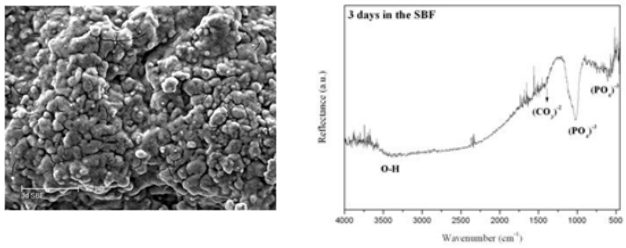


Figure 6. SEM and diffuse reflectance spectroscopy on the infrared applied in samples immersed in SBF for periods of 3 days.

## L 605 CoCr biomedical alloy

The alloy L605 CoCr is widely used for making several types of implants such as bone implants and coronary arterial implants, among others. For coronary applications, it is necessary that tissue growth be suppressed, the product surface be as smooth as possible, since rough surfaces tend to create conditions for cell growth which may be useful in cases where osseointegration is desired but if these artery implants cause cell growth it represents a flaw in its performance. Many properties of cobalt based alloys depend on its crystal structure and the presence of alloying elements such as chromium, tungsten and molybdenum. In most new alloys the amounts of carbon and silicon are controlled (elements considered to be impurities in older alloys). The carbon and tungsten contents influence the amount and type of carbides that form during solidification as the cooling rate and small variations in composition exercise marked influence on carbide formation. The alloy L605, a CoCr alloy was studied. This alloy has about 0.1% carbon and predominantly $M_6C$ carbide, the latter is important in terms of mechanical properties, as it restricts grain growth during annealing and mechanical working.

The material used in this work was developed primarily for stent type intravenous implants. The L605 CoCr alloy is processed in the form of a tube, which is drawn several times until the proper dimensions for the manufacture of implants. The grain size and hardness of the alloy are rigidly controlled due to the influence of temperature on these parameters. The tube is laser cut in a zig-zag form during manufacture of the stent (Figure 7). Once cut, the stents are acid etched, heat treated and polished electrochemically.

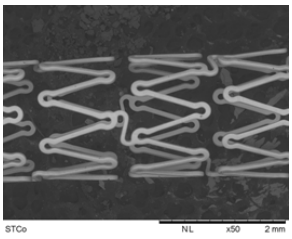


Figure 7. L605 stent.

## Mini-implants for orthodontics

The objective of this research was to evaluate the influence of self-drilling thread and compact thread on primary stability of orthodontic mini-implants - MI (Figure 8a). Forty mini-implants with dual-thread design (compact and self-drilling) were initially examined with a scanning electron microscope. After the screws were inserted in artificial bone (Figure 8b) the insertion torque and load value in the pullout torque or anti-clockwise torque were measured. The torque values obtained using a digital torquemeter were recorded and studied. The results showed that the contact area between the compact thread and bone was higher than the normal thread, due to the smaller thread pitch. The compact thread showed a slight increase in insertion and removal torque in contrast to the self-drilling shape. Nonetheless, the self-drilling thread caused lesser micro damage in the bone. The highest value of insertion and removal torque obtained for the compact thread signified better primary stability, even though it could cause micro damage in the bone, an aspect to be considered regarding osseointegration.

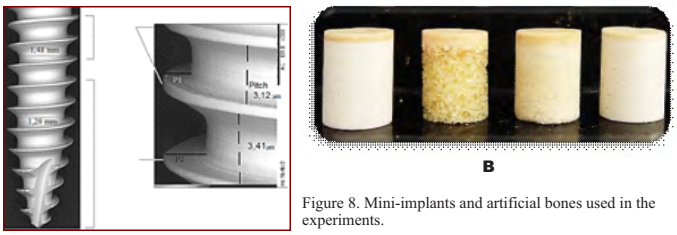


Figure 8. Mini-implants and artificial bones used in the experiments.

## Magnetic hyperthermia

Hyperthermia is considered an alternate method to treat malignant tumors cells and is done by applying heat. Hyperthermia is usually applied to complement other established procedures like radiotherapy and chemotherapy, where tumor temperatures in the range of 313 - 319 K are intended. Magnetic nanoparticles for hyperthemia treatment have gained significant attention in recent years. The magnetic heating occurs by Néel relaxation, Brownian relaxation, and hysteresis loss. Nanostructured Pr-Fe-B powders were prepared by a combination of hydrogenation, disproportionation, desorption and recombination (HDDR) process with high energy milled powders of as-cast alloy ($Pr_{14}Fe_{80}B_6$) and α-Fe (Figures 9 and 10). The produced nanoparticles showed magnetic properties comparable to those reported in hyperthermia studies. Tests of hyperthermia showed that alloy compositions with less rare earth additions (6 at.% and 8 at.%) resulted in higher magnetic heating values (324 K and 314 K), while compositions with 10 at.% and 12 at.% Pr presented temperatures around 311 K and 307 K. Experimentally, the quantification of heat generation from magnetic particles is given by the specific absorption rate (SAR). The specific absorption rates (SARs) of the powders were 201 Wkg$^{-1}$ for $Pr_6Fe_{88}B_6$, 158 Wkg$^{-1}$ for $Pr_8Fe_{86}B_6$, and 114 Wkg$^{-1}$

for $Pr_{10}Fe_{84}B_6$ and $Pr_{12}Fe_{82}B_6$ compositions (Figure 11).

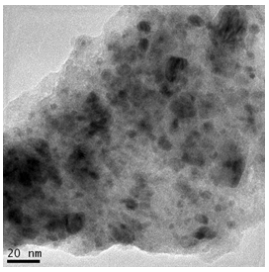


Figure 9. Transmission electron micrograph (TEM) of $Pr_{10}Fe_{84}B_6$ nanomagnetic powders (agglomerated).

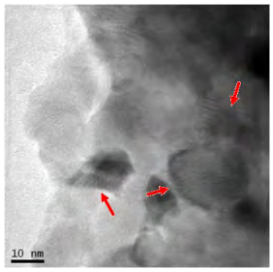


Figure 10. TEM of $Pr_{10}Fe_{84}B_6$ nanomagnetic powders (agglomerated).

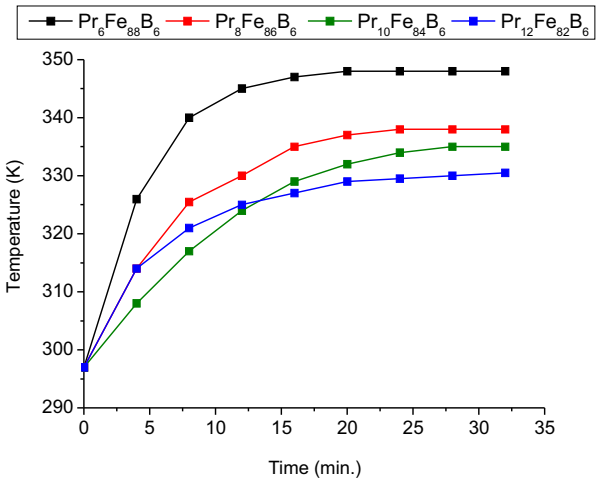


Figure 11. Heating profiles of nanomagnetic powders.

## Nd:YAG laser and mechanically marked biomaterial

Marking techniques are used to ensure identification and traceability of a biomaterial. This study evaluated the influence of laser and mechanical marking on the tribological behavior of ASTM F139 austenitic stainless steel (SS) determining the friction coefficient and wear coefficient in ball-cratering wear tests. The laser marking process was carried out with a nanosecond Q-switched Nd: YAG laser. The cytotoxicity of the marked ASTM F 139 SS was analyzed to determine if the marking process currently used in industry affects the biomaterial's biocompatibility. For comparison, surfaces without marks were also evaluated. A phosphate buffer solution (PBS) was used as the electrolyte. The wear tests were carried out during 10 min with PBS solution. The results indicated that the tribological behavior is influenced by the type of marking process used for this biomaterial, and the wear rate was dependent of the normal force and the kind of sphere. Surface characterization showed microstructure modification due to the high temperatures involved in the laser melting process. An optical micrograph of mechanically engraved biomaterial with a polypropylene ball-cratering mark inside the ring is shown in Figure 12. None of the samples, either marked or unmarked, were cytotoxic, but the laser marked surfaces showed the lowest cellular viability among the tested surfaces (Figure 13).

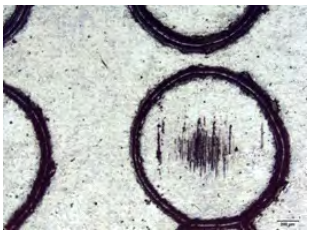

Figure 12. Optical microscopy showing a mechanically engraved biomaterial with a polypropylene ball-cratering mark inside the ring.

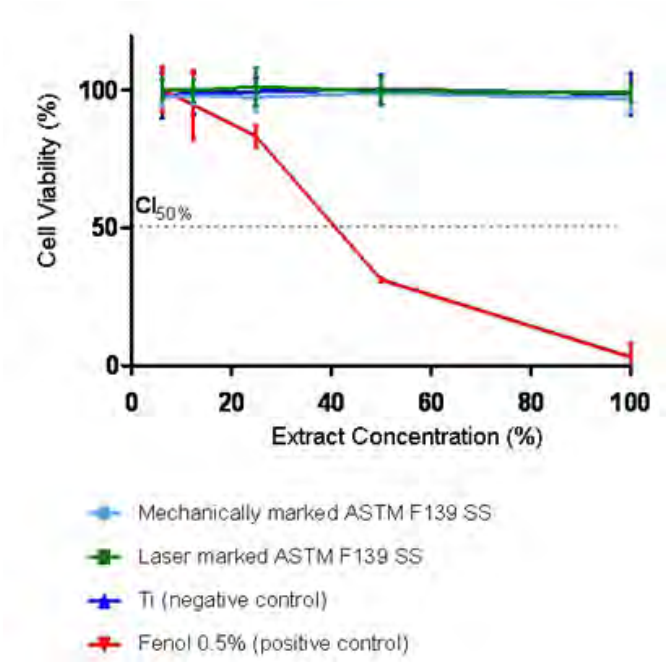


Figure 13. Cell viability for ASTM F 139 SS with mechanical and Nd:YAG laser engravings.

## Femtosecond laser surface treatment of alumina and zirconia bioceramics

Femtosecond laser surface treatment of samples of alumina and yttria stabilized zirconia-alumina composite for deposition and adhesion of apatite was studied. The effects of surface texturing of the different ceramics and the influence of immersion time in SBF 1.5 were studied to determine the optimum conditions to promote the deposition of and the adhesion of apatite on the material's surface. The adhesion of hydroxyapatite is essential for interaction with the substrate and this depends on the properties of material´s surface. The quality of this adhesion will influence its morphology and eventually, the ability for osseointegration. The surface characteristics depend on its chemistry, surface energy and topography. Generally, the reactivity of the surface and surface energy can be affected by wetting characteristics influencing thereby the performance of biomaterials. The adhesion and growth of deposited apatite also depends on surface roughness. The femtosecond laser surface treatment greatly improved the adhesion of apatite obtained by biomimetic coating on the surfaces of materials (Figure 14).

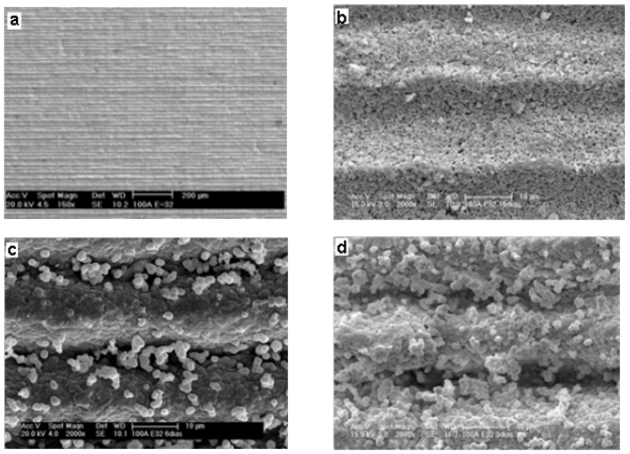


Figure 14. Micrographs obtained by SEM: .Alumina surface (a) and (b) after femtosecond laser surface treatments; (c) and (d) after soaking in simulated body fluid SBF.

### Glass microspheres for selective internal radiotherapy

One of the aims of the Energy and Nuclear Research Institute is to make available radiopharmaceuticals for different therapies. Even though glass microspheres are commercially available for treatment of hepatocellular carcinoma, they are doped with 90Y which is a pure beta emitter. However they are not easily obtained considering the present conditions of the Brazilian Research Nuclear Reactors. We are now developing 165Ho- doped glass microspheres which can be transmuted to 166Ho with potential for application in internal selective radiotherapy (Figure 15). Aluminosilicate and phosphate glasses were investigated for this purpose. 165Ho has the advantage of having a relatively higher neutron capture cross section (64 bars), making the doped glasses suitable for irradiation. Besides that, 166Ho is also a gamma emitter which can provide images of the location of the microspheres in the target region. Irradiation tests are in progress.

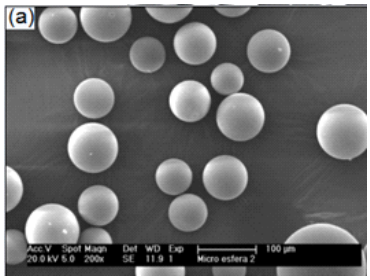


Figure 15. Glass microspheres doped with 165Ho.

The sintering process of aluminosilicate glass microspheres is also being investigated based on differential scanning calorimetry data (Figure 16). For the first time, an endothermic event in the DSC curve could be associated to the sintering process, which was confirmed by changes in microstructure and density increase of the material (Figure 17).

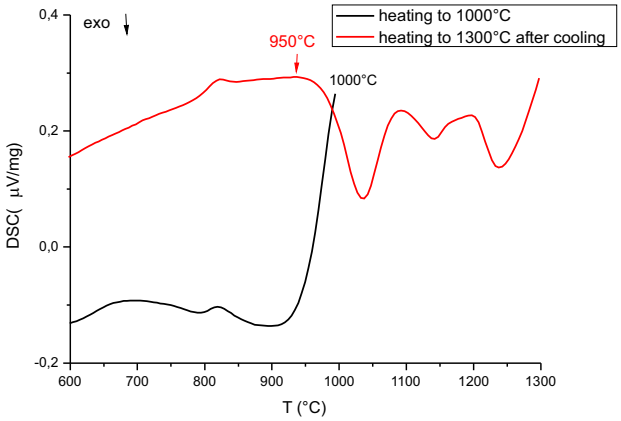


Figure 16. DSC curves of an aluminosilicate glass showing an endothermic event during the first heating, and the lack of such an event in the second heating.

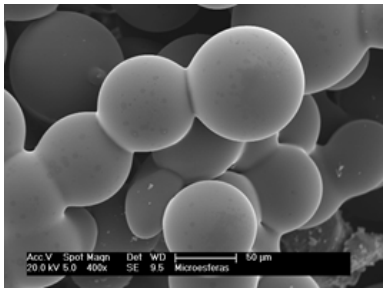

Figure 17. Microstructure of sintered glass microspheres during the heating ramp of a DSC analysis.

### Zirconia and titania dental ceramics

Due to its high biocompatibility, yttria stabilized tetragonal zirconia polycrystals (Y-TZP) is a potential candidate material to substitute titanium implants. The main drawback is its relatively low fracture toughness ($K1c$), especially when compared to metals. However, because of its intrinsic martensitic transformation toughening and associated compressive stresses Y-TZP is currently commercialized as a substitute for metallic implants since it has sufficient mechanical properties to withstand stresses encountered in the oral cavity. In addition, Y-TZP is a white material, and therefore overcomes partially the poor aesthetic aspects of a metallic implant.

Premature degradation of Y-TZP ceramic in aqueous media, referred to as low temperature degradation, is another limitation of this ceramic. This phenomenon has been described in literature for femoral head implants in contact with water or corporeal fluids at temperatures between 100°C and 500°C. This process can be attributed to micro-cracks, resulting in a decrease of its mechanical properties. In our laboratory, Y-TZP dental ceramics were aged using a hydrothermal pressurized reactor to study its tetragonal to monoclinic phase transformation kinetics. In this study, the Rietveld refinement method was used instead of the Toraya equation and this indicated maximum saturation of monoclinic phase of 80% when the Toraya equation was used, compared to 60% with the Rietveld method. Phase transformation as a function of aging time is shown in Figure 18. Therefore the Rietveld method is more accurate because it can evaluate the entire XRD profile, the influence of preferential orientation and the presence of cubic phase.

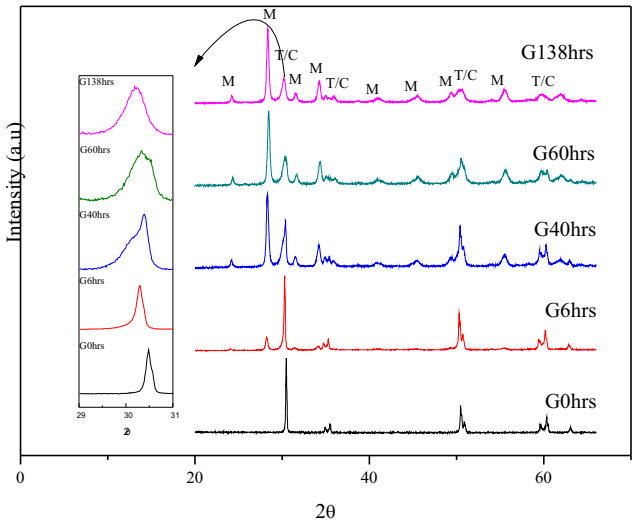


Figure 18. X-ray diffraction spectra of Y-TZP dental ceramics aged for 6, 40, 60 and 138 hours.

Ceramic composites of Y:TZP/$TiO_2$ have also been proposed as a material with potentially higher biocompatibility and these were synthesized by a co-precipitation method and evaluated for application as a biomimetic bone-like apatite layer. The calcium phosphate layer was crystalline in specimens with 30% of $TiO_2$ and amorphous in specimens with 0 and 10% of $TiO_2$. Chemical analysis indicated that this layer was composed of type-A carbonate apatite, which renders good bioactivity as this is also found in bone mineral. The composite with 10% of $TiO_2$ also showed the highest density.

### Polymer composites with ceramics additions

Nowadays, the medical supply industry is focusing on a new segment called smart fabrics for treatment of diseases such as fibromyalgia and poor blood circulation. These fabrics have impregnated particles in the fibers that utilize heat energy emanating from the body to reflect electromagnetic waves in the range of far infrared. Scientifically proven the far infrared stimulates the generation of nitrous oxide which improves blood flow and this helps reduce inflammation and relieves pain. Zinc oxide, besides being an excellent bacteriostatic material irradiates high intensity far infrared when thermally stimulated. The Biomaterials Laboratory at MSTC prepared meters of polyamide 6 fabric impregnated with ZnO microparticles. Figure 20 shows a

scanning electron micrograph of this material.

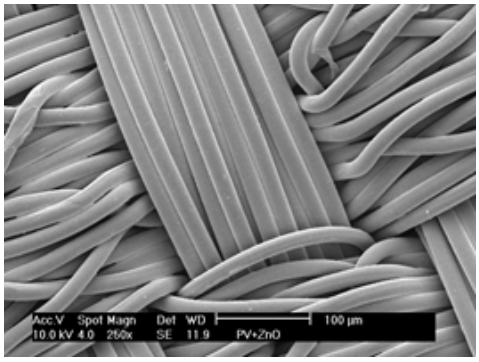


Figure 19. Scanning electron micrograph of polyamide 6 fabric impregnated with ZnO microparticles.

### Thermo-sensitive composites for bone regeneration

Even with the current wide availability of biomaterials, there are some biological conditions that are so severe that only a few of these structures are capable of reestablishing the natural functions of the patient. Thus, substitution of the damaged organ or tissue becomes a more feasible option. Tissue Engineering is a promising multidisciplinary field bridging fields such as biomedical sciences, biophysics and materials science. Briefly, the new tissue or organ is grown by an *in vitro* process which cultivates cells from the patient itself. For growth of the new tissue or organ, it is important to use material that assures structural and mechanical sustentation. Such materials are called *scaffolds* and among all the general properties necessary for its use as a biomaterial, it must also have certain microstructural characteristics, such as porosity, which favor cell mobility and nutrient distribution.

To obtain injectable scaffolds for bone regeneration, the development and study of hydroxyapatite (HA) - charged composites were carried out. Poly-(N-isopropyl-acrylamide) (PNIPAm) was used as the matrix as many of its properties and thermal-sensitivity make it ideal for use as a biomaterial. It has a *Low Critical Solution Temperature* (LCST), around 32°C, and when it is injected at metabolic temperature, it becomes hydrophobic, providing a more mechanically stable and rigid structure to support the bioactive ceramic charge, as well as the new growing tissue.

Through *in situ* radical polymerization (i.e., in HA aqueous suspension), from the monomer N-isopropyl-acrylamide and the cross-linking agent N,N'-methylene-bis-acrylamide, the composite was obtained with different compositions, mainly to evaluate the influence of the HA charge on the hydrogel matrix's properties. Swelling assay was performed in water for the different compositions, so that the mathematical modelling on the diffusion mechanism was evaluated. Scanning Electron Microscopy (SEM) was used to evaluate coupling between the HA charge and PNIPAm matrix, in the different states, i.e., dried and swollen, as shown in Figures 20 and 21.

Regarding the diffusion process, studied through the swelling assay, the mechanisms observed were either fickian or anomalous, governed mainly by network relaxation. The calculated diffusion coefficients $K_s$ of specimens with different HA content and collected at 25°C and 40°C, above and below the LCST, respectively are shown in Figure 22. Below the LCST the magnitude of $K_s$ was higher due to the hydrophilicity, and in other hand lower for temperature above the LCST, due to the hydrophobicity.

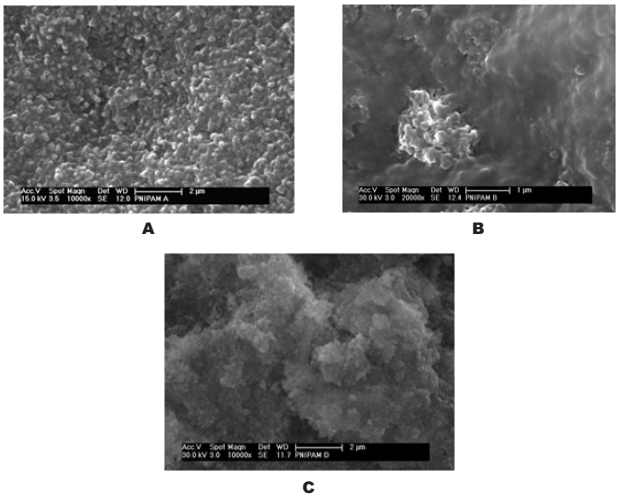


Figure 20. Composites PNIPAm-HA dried, (A) 0%wt HA, (B) 30%wt HA and (C) 70%wt HA.

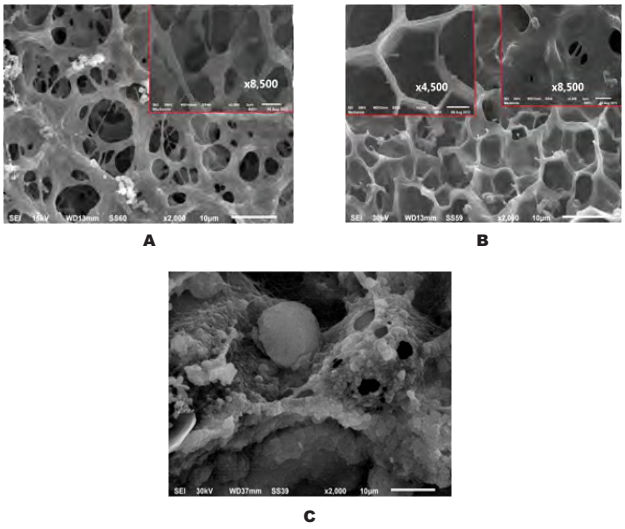


Figure 21. Composites PNIPAm-HA in swollen state (A) 0%wt HA, (B) 30%wt HA and (C) 70%wt HA.

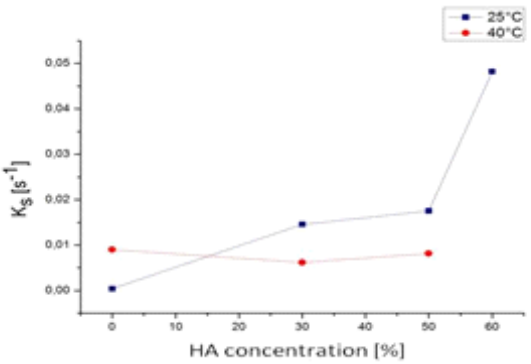


Figure 22. Diffusion coefficient as a function of composition and temperature.

### Ceramic powders synthesized by co-precipitation and solvothermal treatment

The performance and properties of ceramic materials depend strongly on the selection of raw material synthesis process, especially due to the relationship between the powder's physical/chemical characteristics and ceramic's microstructure. Owing to the recent interest in nanoscience and the limitations of the traditional solid state reaction approach for the production of monodispersed nanoparticles with high compositional homogeneity, the use of chemical routes was considered. The main characteristic of these methods is homogeneous mixing of the raw materials at the atomic scale, which successfully promotes diffusion and ensures a lower synthesis temperature. Moreover, the particle size, morphology and surface area of the powders can be controlled. Solution combustion synthesis, coprecipitation, sol-gel, polymer complexation and hydrothermal methods are the chemical synthesis techniques that have been of particular interest because of their simplicity, versatility, and easy scale-up.

In our laboratories, ceramic powders such as stabilized zirconia, alumina, titania, rare earth oxides and hydroxiapatite, have been synthesized by aqueous chemical reactions like coprecipitation. This synthesis in combination with a surface modification treatment, such as hydrothermal or solvothermal processing, can lead to the crystallization and formation of smaller and homogeneously distributed particles at low temperatures. Recently, the use of surfactants such as hexadecyltrimethylammonium bromide, CTAB, has been also incorporated in ceramic synthesis to aid alignment of particles/agglomerates at the interface of solvent and particles, forming micelles and inducing structure reorganization. This procedure has been employed to enhance crystallization of ceramic powders such as nickel oxide-ceria/gadolinia, alfa-alumina and anatase phase in titanium oxide. TEM and SEM micrographs of titania nanotubes and the resulting ceramic are shown in Figure 23 and Figure 24, repectively.

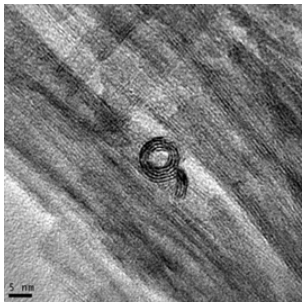

Figure 23. TEM micrograph of titania nanotubes synthesized by coprecipitation followed by hydrothermal treatment.

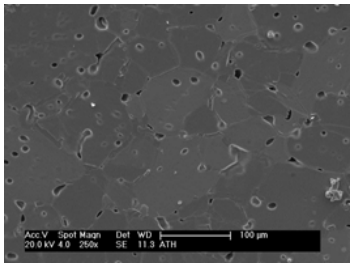

Figure 24. SEM micrograph of polished and thermally etched surface of sintered ceramic of titania synthesized by coprecipitation followed by hydrothermal treatment.

### Nanostructured alumina for $^{99}$Mo-$^{99m}$Tc generator column applications

Tecnecium-99m (metastable 99 tecnecium) is a radionuclide used worldwide in more than 30 million medical diagnosis. It is easily obtained from the disintegration of $^{99}$Mo with β- emission, generating $^{99m}$Tc, that emits gamma rays and disintegrates to $^{99}$Tc. The latter disintegrates to stable $^{99}$Ru. Thus, the $^{99}$Mo-$^{99m}$Tc radioactive couple is formed, in transient equilibrium, considering the high half-life time of $^{99}$Mo, which is 10 times higher than that of $^{99m}$Tc. Methods like chromatography, sublimation and extraction can be used to separate $^{99m}$Tc from $^{99}$Mo. Among these, the chromatographic method is widely used and is based on the strong interaction of $^{99}$Mo (as $^{99}MoO_4^{2-}$ ion) to an chromatographic bed, and the $^{99m}$Tc (as $^{99m}TcO_4^-$ ion) is eluted by a physiologic salt solution.

Among absorbers, alumina is widely used due to its higher absorption of $^{99}$Mo and easy elution of $^{99m}$Tc with 0.9% NaCl solution. The Radiopharmacy Center in IPEN produces generator columns with commercial alumina. However, the material used nowadays still has limited adsorption capacity. This research aims to produce alumina with higher surface area and adequate chemical stability for use in such generator columns.

In recent years, nanometric materials have attracted much attention of researchers due to their properties such as adsorption capacity, which is significantly higher compared to that of conventional forms of the same material. This effect is observed because reduction in particle size leads to higher specific surface area and a higher percentage of atoms are on the surface. This results in more reactive sites.

Nanostructured metallic oxides have high surface area, a morphology rich in defects, small crystalline sizes and high surface reactivity. This allows more metallic ions from solution to be strongly adsorbed. These materials can therefore be used as adsorber materials in generator columns to separate $^{99m}$Tc from $^{99}$Mo.

In this work we employed a low cost mechanochemical method to synthesize γ-alumina with high surface area, which can be employed in the $^{99}$Mo-$^{99m}$Tc generator column. In this method, aluminum nitrate and ammonium carbonate were ground together to produce the alumina precursor (Figure 25A), that were thermally treated at different temperatures, for different periods of time. The γ-alumina phase was obtained after thermal treatment of the precursor at 600, 700 and 800°C, with specific surface areas of 191±9; 321±2 and 286±2 $m^2/g$, respectively. It is important to note the surface morphology of the particles in the SEM images after thermal treatment. The particles present micrometric pores and are covered by very small and irregular particles, that results in the high measured surface area (Figure 25B).

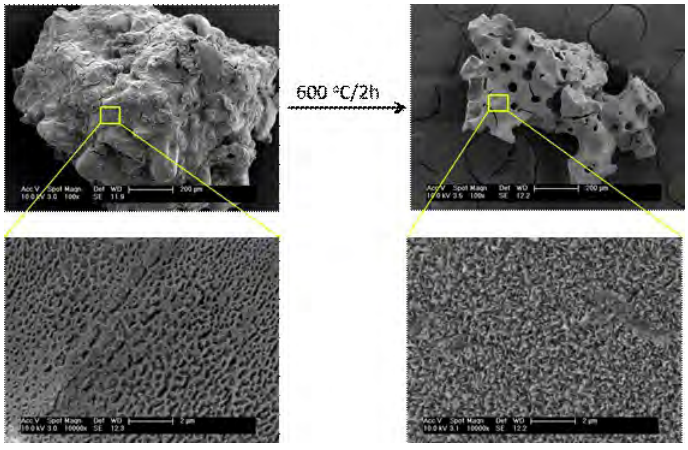


Figure 25. SEM images of (a) alumina precursor and (b) γ-alumina after thermal treatment at 600°C/2h.

### Different synthesis routes to obtain mesoporous ordered alumina

There has been increased interest in obtaining well defined mesoporous aluminum oxides, with high surface area and pore volume. Therefore, significant efforts have been made to produce porous alumina with tailored properties to suit different applications using anionic, cationic or non-ionic surfactants as structure-directing agents.

Many different chemical routes were used to obtain alumina with high surface area. In these different routes a variety of precursors were used: aluminum isopropoxide, aluminum nitrate and $NaAlO_2$. The best results were obtained by the cation-anion double hydrolysis method using P123 and the autoclave step. This method was modified using pluronic F127 and P123 as structure-directing agents, and also using, or not, the autoclave step. A typical synthesis was done as follows: $Al(NO_3)_3.9H_2O$ and Pluronic P123 were dissolved in deionized water, then $NaAlO_2$ solution was added drop wise into the former under agitation. A gel resulted and this was maintained at room temperature for 12h. The gel was transferred to an autoclave and aged at 353 K for

24 h. The gel obtained was washed with deionized water and the solid was recovered by filtration. The resulting solid was calcined at 773 K for 5 h. The nitrogen sorption isotherm of the calcined alumina was typical of type IV, which is characteristic of mesoporous materials. The specific surface area of the calcined sample was 414 $m^2/g$. The calculated pore size for the desorption branch by BJH method has narrow a distribution over the range from 4 to 6 nm and is centered at 5nm, indicating that the mesoporous alumina has uniform pore size and an ordered structure.

### High purity rare earths oxides

Samarium is currently used in many applications, such as catalysts, lasers and metallic alloys. For instance, samarium-cobalt alloys are used to prepare magnets that are resistant to demagnetization. Samarium is also used to absorb neutrons in nuclear reactors, in sensitizers matches, in optical glasses and in carbon arc lamps. In medicine, samarium is used in the form of radioactive $^{153}Sm$ to produce radiopharmaceuticals, which are used to reduce bone pain in patients with cancer. Moreover, new drug compounds containing samarium have been investigated.

The raw material, which was used in the form of rare earth carbonates was produced industrially by chemical treatment of Brazilian monazite. Ion exchange chromatography was performed using a strong cationic resin that is typically employed in water treatment processes to fractionate rare earth elements (REE) without the use of retention ions (Figure 26). Under these conditions, 99.9% pure $Sm_2O_3$ was eluted using the ammonium salt of ethylenediaminetetraacetic acid (EDTA) at a controlled pH. The EDTA-samarium complex was transformed into samarium oxide. The EDTA-samarium complex was transformed into samarium oxide, which was subsequently dissolved in acetic acid to obtain the samarium acetate. Molecular absorption spectrophotometry was used to monitor the samarium content during the proposed process, and sector field inductively coupled plasma mass spectrometry was used to certify the purity of the samarium oxide and the samarium acetate. Typical samarium oxide obtained from the proposed procedure contained the following contaminants in micrograms per gram: Sc (20.90); Y (11.80); La (3.36); Ce (1.87); Pr (1.28); Nd (2.98); Eu (17.70); Gd (84.30); Tb (1.41); Dy (1.92), Ho (2.85); Er (1.49); Tm (2.96); Yb (19.90); Lu (1.18).

The high-purity samarium oxide and samarium acetate produced in this study can be used as an alternative to imported products used in research and development.

Figure 26. Rare Earths pilot plant at IPEN-CNEN-SP.

### Electroceramics

TThe main effort was on research and development of ceramic materials for solid oxide fuel cells and sensors for chemical species. The electroceramics that were studied were yttria- and scandia-stabilized zirconia, gadolinia- and samaria-doped ceria, strontium-doped lanthanum manganite, yttrium- and gadolinium-doped barium cerate and barium zirconate, iron-doped strontium and calcium titanate, calcium and copper-doped titanates. The synthesis techniques for preparing all these electroceramics were solid state reaction, spray pyrolysis, polymeric precursor, peroxo-oxidant, and combustion. The ceramic powders that were obtained were characterized by nitrogen adsorption, X-ray fluorescence, X-ray diffraction, scanning and transmission electron microscopy, and scanning probe microscopy. The pressed powders were sintered either by conventional heating-dwelling-cooling profiles under oxidizing and reducing atmospheres, fast firing, spark plasma, or by two-step sintering. The facilities for carrying out research work on sintered electroceramic pieces are FEG scanning electron microscopy, scanning probe microscopy, dilatometry, impedance spectroscopy over a wide range of temperature (LNT-1500K), frequency (0.01 Hz-140 MHz) and oxygen partial pressures (10 ppm-1 atm).

The highlight of the research carried out was the development of a novel technique for sintering electroceramics at temperatures well below the conventional ones. Figure 27 shows a homemade sample chamber to be inserted in an oven (left) and (right) the positioning of the sample in another experimental setup, which include, for the first time, a dilatometer, an ac power supply and an impedance analyzer.

Figure 28 shows some results related to sintering a zirconia-yttria solid electrolyte (28A) and tin dioxide semiconductor (28B) using the new facility developed at our laboratories. Figure 28A shows that besides the possibility of sintering zirconia-yttria at 800°C (700 degrees lower than the conventional temperature), the ability to choose the desired shrinkage level by adjusting the number of current pulses delivered to the sample. Figure 28B shows how sintering proceeds, depending on the thickness-to-diameter ratio of the specimens.

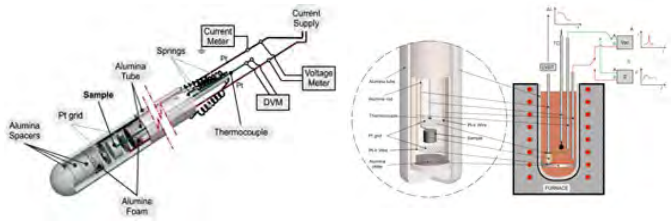


Figure 27. Positioning of a sample for electric field-assisted sintering. Left - homemade sample chamber; Right - modified dilatometer.

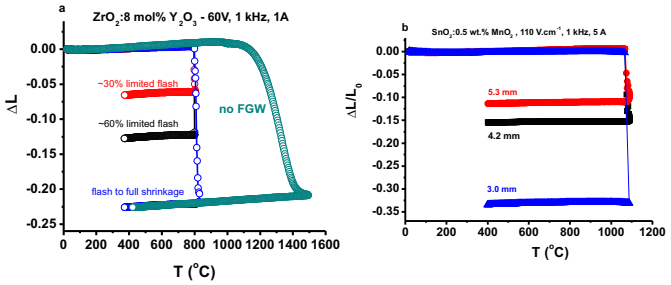


Figure 28. Electric field-assisted sintering (flash grain welding) zironia-8 mol% yttria solid electrolyte (A) and manganese-doped tin dioxide semicondutor (B).

### Structural ceramics

Alumina based cutting inserts provide high abrasion resistance, hardness and chemical stability at high temperatures. This research investigated the feasibility to fabricate high density pure alumina and alumina-polysiloxane ceramics by a two-step sintering process. The first step is carried out to obtain high initial density and the second step consisted in holding at a lower temperature for isothermal sintering to increase the density without grain growth. The addition of polymethylsiloxane (PMS) yielded alumina/$Si_2Al_4O_4N_4$ composites. The sintering studies in nitrogen atmosphere (1650°C/1h) revealed that the highest densities were obtained in specimens with small quantities of PMS. In the case of pure alumina the experimental results revealed that density between 95%T.D. and 99%T.D. could be achieved.

### Microcomposites

Alumina based structural ceramics were developed and refined for cutting tool production. This study investigates the addition of transition metal carbide, such as NbC, TaC and TiC, on alumina sintering and mechanical properties. The oxidation behavior of ceramic materials is very important for structural applications, when materials are exposed to harsh environment or application, for example in the cutting process or as parts for aeronautic industry. In this study the oxidation effect was studied with traditional techniques, as

thermogravimetric analysis of composites in oxidant atmosphere and also with an extended approach of dilatometer technique. It was found spinel type phase when adding transition metal carbides of group V. For the composite $Al_2O_3$:1.5 vol.% NbC was identified the $AlNbO_4$, while for the composite $Al_2O_3$:1.5 vol.% TaC the X-ray diffraction identified phase was $AlTaO_4$, as a result of the oxidation. With microscopic observation was possible to find evidence of liquid formation in grain boundaries for the composite $Al_2O_3$:TaC.

The use of dilatometer under air atmosphere proved to be an effective method to measure the carbide oxidation during sintering tests. With this test it was possible to discover the dimensional changes in composites samples while oxidation mechanisms occur. The experiment demonstrated fast dimensional changes during the formation of $Nb_2O_5$, which lead to breakage of composite at low temperatures. For $Al_2O_3$:TaC and $Al_2O_3$:TiC composites the initial expansion was ~16%, followed by further shrinkage, which suggests that the presence of $TiO_2$ and $Ta_2O_5$ or $AlTaO_4$ are convenient for alumina sintering.

Machining tests of gray cast iron were performed using high cutting speed of 1200 m/min, the tools used were produced with IPEN developed composite $Al_2O_3$:1.5 vol.% NbC and a $Si_3N_4$ commercial tool without recoating. The tool life of the composite in this assay was higher than the commercial tool by ~13%.

The effects of abrasion on the surface of the tools can be seen on alumina tool and on commercial insert of silicon nitride. There was no change in the flank or in the tool geometry, although it was possible to identify small adhesion of iron and abrasion marks on the edge of the two tools, with the micro cracks on the face of both tools.

The machining test with compacted graphite iron, also known as vermicular graphite iron, was performed with cutting speed of 200 m/min. To compare the cutting performance of the composite $Al_2O_3$:NbC were tested two commercial tools, a TiN layer coated cemented carbide tool, and an uncoated $Si_3N_4$ insert. At this test condition the machining performance of the cemented carbide cutting tool was superior to the tested ceramic tools. The developed $Al_2O_3$:NbC insert, having greater chemical inertness showed greater wear resistance than the silicon nitride tool. The surface of the samples was characterized to a greater understanding of the resulting wear on the surface. The alumina composite insert shows signs of abrasion and adhesion of iron on the flank of the tool besides chipping, which is the region of greatest contact with the metal cut. In $Si_3N_4$ tool, the mean flank wear (VB) was greater than that compared to other tools. In both tools ceramic material was no change in the sample geometry. In cemented carbide tool was formed a buildup layer, but this did not alter the flank wear or the flank angles of the tool. The EDS map of this layer showed the presence of some elements such as Fe and Ti.

### Nanocomposites

Containing nanometric inclusions of NbC, synthesized in the laboratory by reactive high energy milling and commercial SiC and $ZrO_2$ are excellent candidates for the machining of hard metals. The sintering was carried under high vacuum and the obtained microstructures were analysed. The results indicated that the addition of carbides modified the sintering behavior, the hardness and fracture toughness were improved by the presence of inclusions. So, cutting tools of alumina containing 5%vol of inclusions were prepared for cast iron machining. Tests were performed to evaluate the behavior of these tools during machining and results showed that these materials showed a high lifetime when machining grey cast iron, leads to a significant increase in the productivity of this material.

### Covalent ceramics

The unique characteristics of silicon carbide allow it to be used in various structural applications, such as, combustion chambers, rocket nozzle, refractory, heating elements, bearings and rotors, heat exchangers, automotive engineering components, cutting tools and applications in the nuclear area. The densification and thermo-mechanical behavior of liquid phase sintered SiC with addition of different molar proportions of $Al_2O_3$:$Y_2O_3$ has been studied. The sintering temperatures chosen for the study are between 1750°C and 1950°C. Regardless of the molar ratio used, mixtures sintered at 1850°C are the ones that showed best relative density performance, around 95%, and mechanical properties such as the Young's modulus, reaching values around 350 Gpa.

The best densification results are obtained with molar ratios of $Al_2O_3$:$Y_2O_3$ between 1:3 and 1:4, and in both mixtures exhibit similar results at different sintering temperatures. Another property that has been studied is the thermal shock resistance of this material, which is evaluated by determining the elasticity modulus after applying the quenching tests. By using this procedure, the material is preheated at a given temperature and rapidly cooled by immersion in water at room temperature. After the first thermal shock cycle at 600°C, the liquid phase sintered SiC has a considerable drop in Young's modulus, though it remained stable after applying the following cycles. The results obtained with the liquid phase sintered silicon carbide with the addition of $Al_2O_3$:$Y_2O_3$ has been shown very promising, and the thermo-mechanical properties are still being studied.

### Aluminum titanate ceramics

Aluminum titanate (AT) is considered to be a potential candidate for high temperature applications because it exhibits low Young's modulus along with very good thermal properties, owing to its crystal structure - isomorphous with the mineral pseudobrookite ($Fe_2TiO_5$). However, the anisotropic behavior of the structure generates localized internal stress which could result in microcracks during the cooling process and consequently in a material with reduced mechanical properties. Also, it is well known that aluminum titanate tends to decompose into alumina and rutile by an eutectoid reaction, making it necessary to stabilize the $Al_2TiO_5$ phase.

Small contents of magnesia and silica have been added to equimolar and non-equimolar mixtures of alumina and rutile to investigate the formation, stabilization, microstructure, sintering and thermal properties of aluminum titanate. Different processing techniques and isothermal treatments have been used to complement research. Results of densification in a dilatometer, differential thermal analysis (DTA) and quantitative phase-analysis by the Rietveld method using X-ray powder diffraction (XRPD) showed that β-$Al_2TiO_5$ formation is favored by magnesia additions because a transitional phase is generated when the $Al_2O_3$- MgO-$TiO_2$ system is submitted to heat treatment. SEM analysis of fractured sample surfaces demonstrated that grains size of $Al_2TiO_5$ decreases with increasing magnesia content. Moreover, non-equimolar mixtures with excess titania might provide complete $Al_2TiO_5$ formation when additions of 1 wt. MgO is used.

### Modification of the polymeric matrix of composites with multi walled carbon nanotubes

The most fragile part of a carbon fiber reinforced polymer (CFRP), is its polymeric matrix. This research proposes a procedure to increase the mechanical properties of the matrix by incorporating carbon nanotubes in the resin. The phenol/epoxy resin used in this procedure has better mechanical properties compared to the pure epoxy, and these properties can be further improved by adding nanoparticles, such as multi walled carbon nanotubes (CNT). Since CNT are chemically stable it is ideal to use microwave heat treatment and a sulfo-nitric bath to create active sites in its surface. Additionally, functionalization of the CNT was undertaken with 3-aminepropyl-tri-ethoxy-silane to aid the adhesion of CNT to the resin. The success of this process was verified by infrared spectroscopy - FT-IR. The phenol/epoxy based resin, modified with these CNT, showed an increase in the glass transition temperature (Tg) of about 10°C, a 20% increase in impact properties and 70% increase in flexural strength. The CFRP obtained using phenol/epoxy resin modified with the CNT showed a 25% increase in the ultimate tensile strength and 68% increase in impact resistance.

In the last three years the main R&D activities were focused on processing and development of multifunction materials: (a) development of technologies and processes as well as management to mitigate environmental impact caused by solid wastes; (b) support efforts to increase energy efficiency, by designing components for fuel cells and porous burners for biogas; (c) use of green technologies to make use of equilibrium diagrams for development of bioglass and composite materials with biocide and biocompatible functions.

## Value addition and mitigation of environmental impacts of industrial wastes

Assessment of reuse potential of all kinds of industrial wastes and by products is nowadays as important as the study of effective inertization of potentially hazardous components present in wastes.

**Assessment of reuse potential of high alumina industrial waste as devitrification aid in common alumina-lime-silica glasses**
In this context, attention was focused on non-metallic slag, known as white dross, produced in the primary extraction of aluminum from ore. Based on the phase equilibrium of the alumina–lime–silica system, the effect of white dross residue (WDR) on the devitrification behaviour of glasses was investigated. The most studied refractory composition, 30WDR, shown in Figure 29, revealed a network of interwoven fine crystals, and this is a typical morphology to be expected for primary nucleation of high temperature aluminosilicates, such as gehlenite. This was confirmed by XRD analysis.

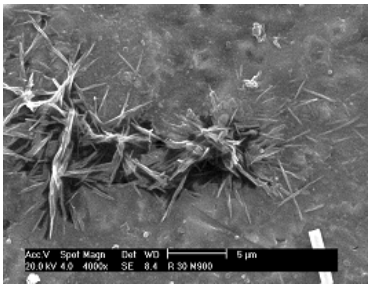

Figure 29. Image (SEM) of fritted glasses containing 30 wt-% WDR (White dross residue) after heat treatment at 900°C for 120 min.

**Galvanic solid waste**
São Paulo in Brazil is considered one of the most populated cities in the word and its eastern regions with the highest population density has many micro and small industries providing electroplating services, especially chromium plating. Solid wastes from these chromium plating companies are usually stored in-house, provoking serious environmental concerns. In this context our group, in collaboration with the Prumo/IPT project has quantified and characterized the solid wastes generated in the electroplating companies and offered technologically safe options for their reutilization, such as incorporation in a glass matrix. The results related to 17 companies and projections for all the facilities are shown in Table I. The chromium plating industry wastes in this region contain mainly Ni, Cr, B, Cu, Ca and S. The galvanic solid wastes were incorporated into frits and glass with satisfactory results. This took care of compounds harmful to health and proved to be an advance, both technically and economically.

**Table I. Values determined for galvanic waste from east zone of São Paulo city**

| Parameter analysed | RSG/year |
|---|---|
| Total amount from the 17 companies | 106 t |
| Average amount from each company | 6 t |
| Estimated total amount in the 30 companies that were given assistance by PRUMO/TS | 190 t |

**Mitigation of wastes from electrical and electronic equipment (e-waste) and reduction of their impact on the environment**
WEEE and RHoS Environment Directives from the European Union were applied to medical equipment and defibrillators. The chemical compounds in different components of medical equipment were identified and quantified and recommendations as per RHoS were made to use those that were environmentally friendlier. New materials such as aventurine glass containing iron and copper, in a wide range of colors, were developed from these residues. These find commercial applications in pigments and as ceramic products for use in the construction industry. This complies with WEEE and is cost effective compared to vitrification of e-wastes. A process to recycle and chemically characterize printed circuit board (PC motherboards) was studied. This process consisted of primary crushing (grinding) of printed circuit boards, particle size classification, separation of metallic and non-metallic elements by using magnetic and electrostatic separators and gravimetric separation using chloroform and bromoform (Figure 30). The metallic and non-metallic elements present were then determined using x-ray fluorescence spectrometry and infrared spectrometry.

Figure 30. Magnetic separator used in recycling of printed circuit boards.

**$Na_2SiO_3$ solution as source of silica**
In the last decade there has been increasing interest in silica nanoparticles based materials, because of their potential use in various applications, such as catalysts, electronic and film substrates, electronic and thermal insulators, humidity sensors, in pigments and pharmacological products. Silica based nanostructured materials consist of interconnected nanosized building blocks. These form highly porous three-dimensional silica network that confer many exceptional properties such as high surface area (500-1000 $m^2/g$), low bulk density (10-200Kg.$m^3$), low thermal conductivity (~0.01W/m.K), high porosity (~99%), high optical transmission (99%), low dielectric constant (~1.0-2.0), low refractive index (~1.05) and low sound velocity (100m/s). Alkoxides precursors can be substituted by cheaper and water soluble precursors such as $Na_2SiO_3$ (sodium silicate or water glass) for sol-gel processing. This study proposes a simple, cost effective and environment friendly process to obtain nanostructured silica spheres by using sodium silicate, a waste matter derived from alkali fusion of zircon sand, as a source for silica and a tertiary amine ethoxylate as a surfactant template agent. Silica sol was obtained by hydrochloric acid-catalyzed hydrolysis reaction with $Na_2SiO_3$. Homogeneous spherical particles of silica with SSA (specific surface area) in the range 200 - 960 $m^2\ g^{-1}$ were obtained. SEM micrographs of silica particles are shown in Figure 31.

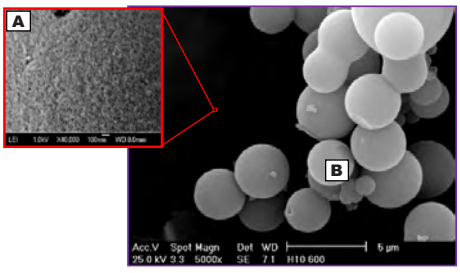


Figure 31. SEM micrographs of the silica particles with SSA=961.54 $m^2g^{-1}$. (A) surface of the particles; (B) morphology.

## Development of new structures for improving energy generation efficiency

### Microstructure design using MA and SAS as processing routes for multi-layered cermet materials

Mechanical alloying has been successfully used to prepare cermet materials in which different metallic layers have been plated with ceramic particle agglomerates. In zirconia-nickel based materials, the layers were designed to improve catalytic and reforming capabilities. Sequential milling steps can place molybdenum and other refractory metals with interposing Ni and Cu layers to avoid alloy formation. This special processing method increased Cu activity up to a proper level for repulsing C poisoning on the catalyst. SEM and TEM analysis of sintered pellets confirmed that Cu and Mo precipitated near the pores, while thermo gravimetric and DTA studies coupled with mass spectrometry demonstrated that the strategy to avoid poisoning was valid.

### Colloidal processing

One of the challenges in this area is to understand the viscoelastic behavior of particulate suspensions. This important step in powder processing is still little understood. Viscoelasticity is related to flow behavior in processes such as injection and extrusion, and it can be determined by oscillatory rheological measurements and with curves of creep-recovery. Due to the inherent difficulties in preparing ceramic suspensions with more than 80 wt% of solids and in making measurement, viscoelasticity of ceramic suspensions is virtually unknown, and thus the aim of this research was to investigate the viscoelastic behavior of stable alumina suspensions with high concentration of solids. The transition shear-thinning to shear-thickening, with increasing solid content displaced to lower shear rates (Figure 32), starting at a shear rate of 50 $s^{-1}$ in suspensions with 43 vol.%. This change is similar to that observed for kaolin concentrate suspensions. The increase in viscosity observed in kaolin suspensions from 400 $s^{-1}$, is attributed "house of cards" structure formed by the difference in the electrostatic charge between the edges and faces of kaolin particles, which have a platelet shape. In the alumina suspensions, this behavior was attributed to lamellar morphology of the alumina particles, and the particle size (0.67 μm), associated with high solids concentration.

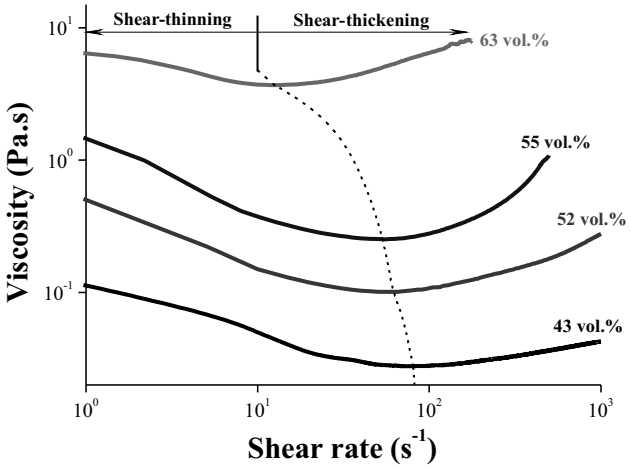


Figure 32. Viscosity curves versus shear rate highlighting the transition, shear thinning to shear thickening, for alumina suspensions with different amounts of solids.

### Burned gas for lightning processing by replica

Renewable energy sources are the only alternatives to provide widespread access to energy, from the United Nations Organization's (UNO) point of view. On the basis of this, it is essential to develop materials that help save energy, like porous ceramics that combine light weight with high mechanical strength. In this context effort are ongoing to improve the homogeneity of pore size distribution in porous yttria ceramics by evaluating its morphology during replica processing. Based on our previous work about the rheological behavior of suspensions, aqueous yttria suspensions with 30vol% of solids ($S_{Y30}$) were prepared and immersion conditions as well as heat treatment optimized. The effect of IT on morphology of sintered yttria nettings ($N_Y$) is shown in Figure 33. No cells were trapped, and our observations confirm that the rheological behavior of the suspension was suitable. Subsequent results showed that this interval did not render favorable conditions to cover the surface of Ncs uniformly.

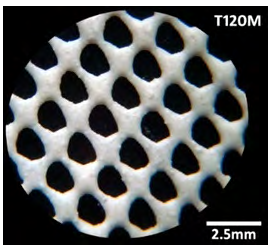


Figure 33. $N_{Y_s}$ produced by replica, whereby $I_T$ 120min.

## Equilibrium diagrams for multifunction materials development

Design and development of new chemical compositions based on thermodynamic concepts and the use of equilibrium diagrams is one of the main interests of this research group. In this context, in the last three years we studied new compositions focused on functional bioactivity.

### A step towards a "Green Universal Biocide"

An important research activity of our group in the field of inorganic biocides is related to nanoscience and nanotechnology, specifically materials supporting silver or copper nanoparticles. Several authors have pointed out the negative effect of metal nanoparticles on human health. Our research is focused in a different direction, the study of biocide activity of a series of soda-lime glasses with increasing calcium oxide content. The soda-lime glass powders (d<100 microns) with CaO content in the range 15 to 20 wt-% are strong inorganic biocide agents, with a logarithm of reduction >4, versus Gram-positive and Gram-negative bacteria, and yeasts (Fig.34A-I series), as shown and explained in Figure 34.

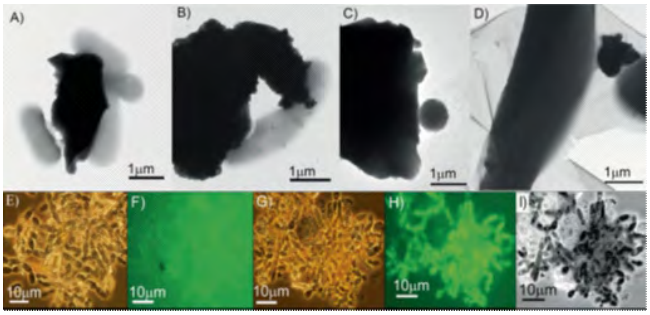


Figure 34. Biological activity of the glass samples against cell cultures. Top frames: TEM micrographs after 1 h of biocide test showing: E. coli culture supplemented with G-3 (A) or G-4 (B); M. luteus culture supplemented with G-3 (C) and C. krusei culture supplemented with G-3 (D). Bottom frames: Optical micrographs corresponding to a culture of C. krusei after 1 h supplemented with: G-1 under phase contrast light (E), G-1 under fluorescence conditions (F), G-3 under phase contrast light (G), G-3 under fluorescence light (H) and superimposed micrographs (G-H), where the black colour cells correspond to dead cells. Optical superimposed micrographs corresponding to a culture of C. krusei under phase contrast light superimposed to the micrograph under fluorescence conditions after 1h supplemented with: G-1 (E) and G-3 (F).

Moreover in another direction, we developed bioglass/hydroxyapatite composite ceramics. The crystalline phosphate phase (OCP) on the surface of the sintered material after immersion in SBF (Simulated Body Fluid) (72h/38ºC) was observed and it indicated bioactivity of the material (Figure 35).

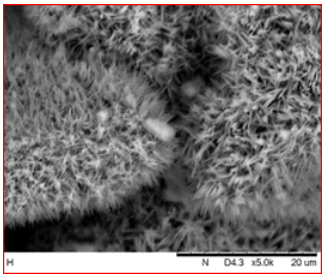

Figure 35. Crystalline phosphate phase growing on glass matrix surface after immersion in SBF. (72h/38ºC).

### Fracture mechanics of cracks

Grinding ball mills are used in mining plants and are also used in the initial stages of the uranium fuel cycle. Depending on a number of factors, such as inappropriate design, manufacturing, overloads, poor maintenance and inadequate operating procedures, defects develop in the structural components of this equipment. The structural components of a mill include the shell, heads and trunnions. These components are expensive, have lead times for fabrication and delivery which could vary from two to three years, depending on market demand. Consequently, it becomes increasingly necessary to properly evaluate defects in these components. The aim of this work was to analyze the fracture mechanics of cracks observed in the structural components of large equipment such as the ball mill and compare it with theoretical values of crack growth rate. This was done through periodic inspections performed on this equipment. The defects to be analyzed are cracks observed in the trunnion, typically made from nodular cast iron (Figure 36).

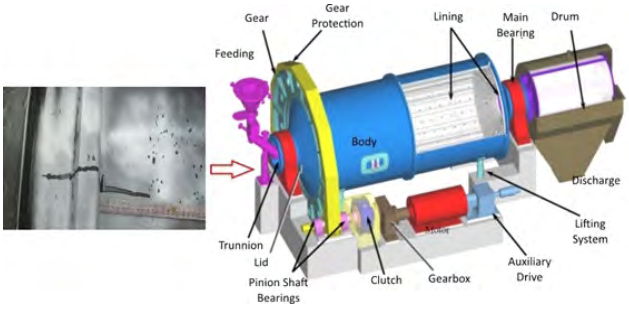


Figure 36. Cracks in trunnion of grinding ball mill.

### Mechanical spectroscopy - dynamic mechanical analysis

Dynamic mechanical analysis consists of applying cyclic and controlled stress or strain in a sample followed by measurement of the strain or the resultant stress respectively. By varying the frequency of the applied force and temperature it is possible to determine mechanical properties such as elastic modulus and damping coefficient of a particular material under thermal and time spectrum.

This form of mechanical spectroscopy analyzes the internal friction and, depending on the nature of the material being studied, its viscoelastic behavior. These parameters enable indirect determination of processes taking place, down to the atomic level, in solid solutions, phase transformations, the structure of defects such as crosslinking, dislocations, dynamics of atoms (interstitial and substitutional), at grain boundaries, damages caused by thermal effects, radiation and the presence of hydrogen. Determination of mechanical phenomena such as creep and relaxation beyond the damping capacity of the material are also possible.

The latest studies that have benefited from the DMA include: (a) evaluation of molecular and mechanical changes in bone matrix caused by ionizing radiation using complementary techniques of analysis like infrared spectroscopy and mechanical testing; (b) study of the effect of zirconium and niobium content on the mechanical properties of the ternary alloy Ti-Nb-Zr after different processing conditions and heat treatments; (c) determination of the modulus of elasticity; (d) study of biomaterials and biological materials; (e) determination of viscoelastic properties of polymers and their glass transition temperatures.

Our laboratory has a Netzsch DMA 242 with the following capacities: temperature range: -170°C to 600°C; static or dynamic atmosphere (air, inert gases); deformation mode: three-point bending, single and dual cantilever bending, linear shearing, compression/penetration, tension, creep, relaxation sweep modes (strain sweep or stress sweep); modulus range (E') $10^{-3}$ MPa - $10^{6}$ MPa (depending on deformation mode); frequency range: 0.01 Hz - 100 Hz up to 25 fixed frequency steps; force range ± 0.002 N - 8 N; 8 N max. proportional or constant static pre-force; max. total force: 16 N; force resolution 0.0005 N; amplitude range ± 0.1 up to 240 µm; amplitude resolution 0.0005 µm. Figure 37 shows our equipment.

Figure 37. DMA equipment.

### Aluminum alloys for automotive applications

Automobile parts made of steel/cast iron have been replaced with those made with aluminum alloys to not only reduce weight but also to reduce fuel consumption the emission of pollutants. Structural materials require not only high strength/weight ratio, besides reasonable cost, but also high fatigue resistance. Moreover, the Al alloy parts have a rather high residual value, because the aluminum is fully recyclable at the end of the useful life of the part. Automotive cylinder liners are mechanical components with the function of being an internal coating of automotive engine cylinders. Among the different foundry casting methods, the centrifugal casting technique relies on a tubular die with a high rotational speed during pouring (1,000 to 1,500 rpm). The dynamic effect of the high rotational speed promotes high centrifugal acceleration, reduces porosity and promotes some density segregation effect that cannot be achieved in static foundry processes.

The centrifugal casting process using the Al-Si alloys for cylinder liners can induce some reduction in the silicon content, mainly with low hypereutectic compositions compared to the materials used in static processes. The high centrifugal acceleration prompts silicon to run mainly in the inner diameter direction, due to its lower density compared to that of the aluminum alloy, even in the liquid state. Thus, with low silicon content on the outer side, it becomes easier to guarantee wear resistance in the cylinder/piston and ring working surfaces, as well as the mechanical properties requirements Extruded aluminum alloys find applications as automotive components. For automotive components, adequate mechanical strength/weight ratio at a reasonable cost is essential. Moreover, these materials should be resistant to fatigue when used as components exposed to cyclic loads. Precipitation strengthening, in which precipitates form within the matrix phase, is an important hardening method and is used to increase the strength of some aluminum alloys. Shot peening is a process to cold work the surface and is used to increase the fatigue life. This can be evaluated by residual stress measurements.

### Welded joints

Welded joints with suitable mechanical and metallurgical properties were studied and developed for various applications. The difficulties encountered in the area of oil and natural gas exploration in ultra deep waters are related to mechanical properties and corrosion resistance of various components. Internal corrosion of AISI 8630 tubes can be minimized by coating it with nickel alloy 625 (inconel 625®) using GTAW (Gas Tungsten Inert Gas) or TIG (Tungsten Inert Gas) welding processes. However this could lead to formation of embrittling phases in base material AISI 8630, the cladding material, nickel 625, or at the interface between these dissimilar materials.

Hence, post weld heat treatments (PWHT) must be performed to minimize formation of the martensitic phase during weld cooling. This PWHT could however cause brittle phases to form. The hardness test values near the weld region indicated that hardening was due to diffusion of elements from the cladding material to the low alloy steel. Figure 38 shows areas denominated as Partially Diluted Area (ZPD) that reduced impact resistance. EDS analysis showed variation in the

amount of alloying elements along the joint.

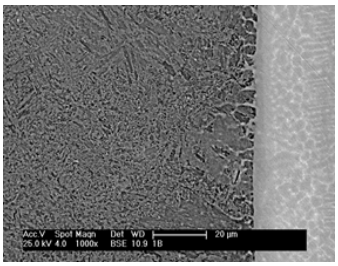

Figure 38. Scanning electron micrograph showing variation of alloying elements along the joint. Base material (MB) - AISI 8630 with cladding material (MA) - alloy nickel 625.

Welding is an important step in the manufacture of subway cars, mainly structural components and finished surfaces of passenger cars using stainless steel AISI 301 L. Welded joints can have discontinuities that affect the mechanical and metallurgical properties of the weld. The presence of these discontinuities, depending on their size and nature or both, may lead to rejection of the welded component based on either reduction of mechanical properties or not satisfying acceptance criteria.

A component that has been rejected for either reason attributable to the presence of discontinuities can be retrieved by reworking the joint. Re-melting of the weld using the TIG (Tungsten Inert Gas) process without the use of filler material is a technique that can be used to repair the component. This study evaluated the influence of the TIG welding rework process on mechanical behavior and microstructure of welded joints by means of mechanical tests, non-destructive testing and microstructure characterization of the weld. Figure 39 shows the fracture region of a specimen after a tensile test and reveals that rework did not change the mechanical behavior of repaired welded joints. However, removed of the reinforcing can modify the mechanical properties of the joint.

Figure 39. Specimen with a reworked weld joint following a tensile test.

Overlapping joints of 350 maraging steel were welded using the fiber laser process. The welded joints were evaluated by a tensile shear test, Vickers microhardness measurement and microstructure characterization at various regions. The results indicated that the conditions used in laser welding were adequate to obtain the required amount of weld penetration. There was an increase in the Vickers hardness in the heat affected zone but this did not affect the results of the tensile shear test. Figure 40 shows the fiber laser welded joint.

Figure 40. Macrographic image of the fiber laser welded joint.

A variety of techniques are available to deposit coatings with different chemical compositions and microstructures to obtain surfaces to with properties such as increased resistance to oxidation, wear, erosion, corrosion etc., and quite distinct from that of the substrate's properties such as toughness and tensile strength. This combination of specific properties of the substrate and that of the coating has been exploited and several coatings are being developed at the Materials Science and Technology Center in IPEN.

### Zinc oxide thin films for solar cells

Zinc oxide (ZnO) is an important n-type semiconductor material. It is environment friendly, inexpensive and non-toxic. ZnO can be used in many opto-electronic devices due to its physical characteristics such as high binding energy, direct wide band gap, high electrochemical stability and good optical characteristics. ZnO can be grown as thin films with different morphologies and each morphology is suitable for making sensors or devices like thin-film dye-sensitized solar cells, gas sensors, piezoelectric transducers, surface acoustic wave filters etc. A new route to grow ZnO seed layer was developed using the SILAR method. This method - Successive Ionic Layer Adsorption Reaction (SILAR) was developed to deposit ZnO seed layer on to $SnO_2$ coated glass plates. This technique consists of sequential immersion in various baths to synthesize nanorods and nanocrystallites of ZnO for use in thin-film solar cells. This technique enables time, temperature and agitation of a sequence of chemical baths to be computer controlled. ZnO nanorods, shown in Figure 41, were obtained and these permit higher solar-to-electric energy conversion efficiencies.

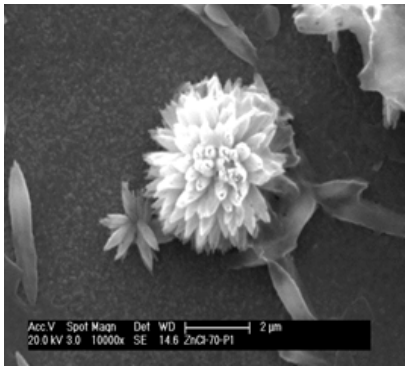


Figure 41. ZnO nanorods on a tin oxide surface.

### DLC coatings for friction reduction

In the last few decades concerns related to emission levels from internal combustion engines and reduction of fuel consumption have been debated at many global forums with clear deployments in more restricted specifications to allow commercialization of new internal combustion engines. Even with the introduction of new technologies the engines still present significant energy loss due to mechanical friction. One of the main contributors to friction in an engine is that in the piston-piston ring-cylinder liner system and this has been the focus of many investigations with the aim to reduce engine friction losses. The properties of Diamond-Like Carbon films (DLC) such as superior wear resistance and low friction coefficients are well known and makes them suitable for many different tribological applications. We evaluated the application of a graded amorphous DLC film over the running surface of a cylinder liner. The coatings were deposited by the plasma assisted chemical vapor deposition process (PACVD), as the alternative solution, to reduce engine friction and thereby reduce brake specific fuel consumption (BSFC) and improve wear resistance behavior of the piston rings and cylinder liner contact surfaces as well. Parts without an inner DLC coating and DLC coated parts with similar running surface roughness were compared in reciprocating bench tests. The tests showed a 19% reduction in the coefficient of friction (COF). In a same trend, fired gasoline and diesel engine tests showed a friction mean effective pressure reduction (FMEP) of 12% and small brake specific fuel consumption (BSFC) of up to 2.5% at low engine speed range respectively.

### Niobium based films for improvement of corrosion resistance

AISI 316 stainless steels are used in various industrial applications such as pumps, condensers and in many aggressive atmospheres. However, the presence of chloride ions increases their susceptibility to pitting corrosion and cracking. Improvements in corrosion resistance of these steels can be achieved through the use of coatings. This research addressed the electrochemical behavior of niobium based thin films deposited by magnetron sputtering on AISI 316 stainless steel substrates. Two routes were developed: metallic niobium coatings and niobium pentoxide coatings. The metallic coatings were deposited over unheated substrates and those heated at 200°C for 3, 5 and 10 minutes. The niobium pentoxide coatings were deposited at room temperature. The concentrations of niobium and oxygen were evaluated by Rutherford backscattering spectroscopy. The results showed that the composition of these films is near $Nb_2O_5$. The corrosion behavior of the specimens was evaluated by means of electrochemical impedance spectroscopy and potentiodynamic polarization using a 3.5 wt.% NaCl solution at room temperature as the electrolyte for an immersion period of 19 days. The results indicated higher corrosion resistance when the niobium film was deposited on the heated substrate, and that a longer deposition time produced more protective films. Better results were obtained when niobium pentoxide coatings were used.

### $TiO_2$ thin films for improvement of corrosion resistance

The metal organic chemical vapor deposition (MOCVD) process was adapted and/or developed to produce a variety of coatings to protect various metallic materials exposed to different aggressive environments. The coatings include CrN, $Cr_2O_3$, $TiO_2$, TiN. The effect of $TiO_2$ films obtained through the MOCVD technique on the corrosion resistance of the AISI 304 stainless steel was investigated. The films were deposited on substrates held at two different temperatures: 300ºC and 500ºC. The corrosion behavior of the coated specimens was evaluated by means of electrochemical impedance spectroscopy (EIS) and potentiodynamic polarization using a 3.5 wt.% NaCl solution at room temperature as the electrolyte for an immersion period of 14 days. The morphology of the films was assessed by electron scanning microscopy. The results indicated that the film obtained at 300ºC provided better corrosion resistance while that obtained at 500ºC presented limited corrosion protection. This behavior is due to the influence of both morphology and thickness of the films which depend on the deposition temperature.

### Hydrocalcite coatings for increased corrosion resistance

A room temperature chemical coating process was developed to coat Al alloys with hydrocalcite (HTC). Field tests were carried out in which dummy MTR fuel plates were coated with HTC and with HTC modified with Ce and exposed for extended periods to the spent fuel basin of the IEA-R1 reactor. The tests revealed that coated plates were free from any form of corrosion compared with uncoated plates. This reveals the immense potential of HTC + Ce coatings to protect spent Al-clad fuel elements against corrosion during extended wet storage. Figure 42 shows HTC coating on an aluminum alloy surface.

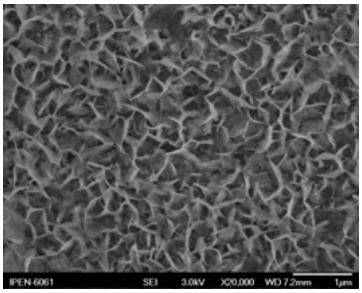


Figure 42. HTC coating on Al alloy surface.

### High temperature degradation resistant coatings

The high temperature oxidation behavior of two ferritic stainless steels in synthetic air and argon at 850-950°C was determined. This study was undertaken to obtain feedback to ascertain use of this steel as interconnects in solid oxide fuel cells (SOFC). The high temperature oxidation and erosion-oxidation (E-O) behavior of nanostructured $Cr_3C_2$-25(Ni20Cr) coatings on AISI 310 stainless steel was determined. An overall 50% increase in E-O resistance of the nanostructured coatings, compared with the microstructured coating, was observed.

The thermodynamic properties of nanocrystalline $Cr_3C_2$-25(Ni20Cr) and WC-12 Co powders were determined to increase understanding of the microstructure and physical properties of these materials when used as coatings to protect other metallic materials exposed to severe environments. The high temperature thermal stability and mechanical properties of nanostructured WC-Co coatings were determined. Optimization of the use of different rare earth (RE) oxides as coatings to further enhance the high temperature oxidation resistance of chromium dioxide forming Fe-Cr alloys has been done. This optimization was achieved taking into consideration the nature of the RE, RE oxide crystallite size, RE oxide morphology, ionic radius of the RE and the RE oxide coating coverage. Marked improvements in alloy oxidation resistance at 1000°C and 1100°C were observed.

### Niobium coatings for improved sulfidation resistance

There are many industrial processes where metals are exposed to gases under high temperature. These gases may consist of a single gas like oxygen or complex mixtures of oxidizing gases such as $H_2S$, $SO_2$, $CO_2/CO$ and $H_2O/H_2$. These processes include oil refining, coal gasification and conversion of fossil fuels. The study of the sulfidation behavior of coatings to resist these gaseous atmospheres in the existing micro - power plants is especially important to extend the life of metallic components. The search for alloys and coatings that allow formation of sulfides at low growth rates has stimulated studies in this area, particularly reactions involving refractory metals such as niobium and molybdenum. The goal of this study was to investigate the effect of a niobium coating on the isothermal sulfidation behavior of FeCr alloys at 500º, 600º and 700°C.

### High temperature behavior of Ti-6Al-V alloy and nickel-based superalloys

Ti-6Al-4V alloy and nickel-based superalloys have found applications at elevated temperatures in aggressive environments. The alloy Ti-6Al-4V is one of the most widely used titanium alloy because of an excellent combination of properties like strength, toughness, corrosion resistance and chemical stability. Inconel is a nickel-chromium-molybdenum superalloy with high corrosion resistance and strength at elevated temperatures. Surface modifications of Inconel and Ti-6Al-4V have been carried out to improve mechanical properties at elevated temperatures. Creep and hot tensile tests were performed to evaluate the mechanical properties at elevated temperatures. The surface modifications that were carried out were plasma immersion ion implantation (PIII), thermal oxidation and plasma nitriding.

The influence of oxidation of a Ti-6Al-4V alloy at 800°C on its tensile properties at 600°C has been studied. Specimens of this alloy were oxidized at 800°C for 0.5, 1, 5, 10, 20 and 40 h. Subsequently, tensile tests were carried out at 600°C and the fracture surfaces were examined. Oxidation of the specimens resulted in formation of an oxide layer that spalled and another oxide layer that adhered to the substrate. Oxide formation increased with increase in duration of oxidation. In this investigation, density curves of the oxide layer as a function of duration of oxidation at 800°C were used to identify a parabolic oxide growth law. The results of this study revealed coherence between the experimental data and calculations based on the Pilling-Bedworth law. The mechanical strength of the Ti-6Al-4V alloy did not vary significantly with oxidation, but reduction in cross sectional area with increase in oxide layer thickness, as well as the slope of the stress-strain curve decreased beyond the ultimate tensile strength. Fracture of the tensile tested specimens was predominantly ductile with microcavities. At certain regions of the oxide layer, brittle fracture with radial cracks was observed indicating intergranular fracture. The aim of the nitrogen Plasma Immersion Ion Implantation (PIII) treatment was to improve the mechanical properties of the Ti-6Al-4V alloy surface. The selected alloy after ion implantation by plasma immersion was submitted to creep tests at 600ºC, in constant load mode at 250 and 319 MPa. The techniques used in this study were optical microscopy and scanning electron microscopy. Fractographic analysis of the creep tested samples showed necking and microcavities. The creep results revealed a significant increase in material strength. This treatment can be used for oxidation protection at high temperatures.

Superalloys were developed for use at high temperatures, where severe mechanical stresses are encountered, and high surface stability is frequently required. Improvements in surface properties of a wide range of alloys have been achieved by implantation of nitrogen. Field test results with industrial tools and components from a diverse range of applications have been encouraging. The objective of this study was to improve the mechanical properties of Inconel 718 surface using PIII (Plasma Immersion Ion Implantation). Expansion of the fcc lattice after a three-hour implantation was observed from x-ray diffraction (XRD) data. The best result was achieved in samples that were treated for 3 hours. These samples presented very little wear after 5000 cycles in an unlubricated pin-on-disk test. Another on-going study is determination of creep behavior of double aged superalloy Inconel 718. Initially, a solubilization treatment was performed at 1095°C for 1 hour, followed by a double aging treatment at 955°C/1h - 720°C + 620°C/8h C/8h. The alloy was submitted to creep tests in constant load mode at 650, 675 and 700ºC. The results of this double aging treatment indicated an effective change in microstructural characteristics such as increased hardness and grain size, improved distribution of precipitates after heat treatment, which proved to be a more effective barrier to the movement of the defects in the crystalline lattice.

### Batteries and supercapacitors materials development

Significant progress has been made in our laboratories in R&D activities related to batteries and supercapacitors materials. This consisted mainly of studies related to electrodes for these devices. Over the past years, international research has concentrated on the study and improvement of supercapacitors materials. These electronic devices are used for storing energy over time periods ranging from seconds to several days. The main factor determining the energy storage duration of a supercapacitor is its self-discharge rate. This property relates to the gradual decrease in electric potential that occurs when the supercapacitor terminals are left unconnected to either a charging circuit or an electric load. The self-discharge and lifetime of supercapacitors are dramatically affected by small variations in room temperature. Self-discharge is faster with increase in room temperature. The temperature inside electronic devices can vary considerably during continuous operation and can affect sensitive components. Electric materials based on activated carbon supercapacitors have been studied in our laboratories in terms of temperature dependent properties.

The microstructure and properties of materials based on Pr-La-Al-Mg-Mn-Co-Ni alloy for NiMH batteries have also been studied in our laboratories. These electric materials were produced using the pulverization process and a standard powder metallurgy route. Measurement of properties was carried out using standard techniques to characterize electric equipment.

### Hydrogen absorption in $LaNi_5$ based alloys for nickel metal hydrides batteries

Over the past years, $LaNi_5$-based hydrogen storage alloys for use in electrodes of rechargeable batteries have systematically incorporated specific alloying elements to improve the kinetics of hydrogen absorption and desorption, increase cycle life, improve corrosion resistance, etc. Cobalt, aluminum, manganese and magnesium are invariably present in the alloy. A specific composition, $La_{0.7}Mg_{0.3}Al_{0.3}Mn_{0.4}Co_{0.5}Ni_{3.8}$, showed 337.1 mAh/g as maximum discharge capacity. Cobalt is a very important element to improve the discharge capacity and extend the cycle life of the electrode alloys, but recycling and reuse of cobalt is an environmental problem. Several examples of Co-free and low-Co $AB_5$ type alloys can be found in the literature.

On the basis of this information, it is considered that a systematical change in the composition of $La_{0.7}Mg_{0.3}Al_{0.3}Mn_{0.4}X_{0.5}Ni_{3.8}$ (X = Cu or Sn) alloys can improve discharge capacity, cycle life, corrosion resistance and microstructure. Figure 43 shows the SEM micrograph of $La_{0.7}Mg_{0.3}Al_{0.3}Mn_{0.4}X_{0.5}Ni_{3.8}$ (x = Cu, Sn) hydrogen storage alloys.

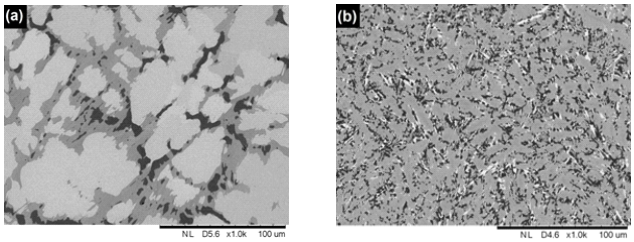


Figure 43. SEM micrograph of the $La_{0.7}Mg_{0.3}Al_{0.3}Mn_{0.4}X_{0.5}Ni_{3.8}$ alloys: (a) X=Cu and (b) X=Sn.

### Materials for magnets

(Nd, Pr)-Fe-B-based sintered magnets are currently the most widely used high-performance permanent magnets. Sintered magnets reveal a microstructure composed of $Nd_2Fe_{14}B$ grains, a small fraction of Nd-rich grains and possibly a thin Nd-rich grain boundary layer. To further improve the coercivity of commercial magnets, it is essential to obtain a better understanding of the mechanism of coercivity increase caused by post-sinter annealing that is currently in use. Dysprosium (Dy) is a strategic rare-earth element with many uses in high- tech industries and supply of this element is extremely limited. By replacing the element neodymium (Nd,Pr) with Dy, the (Dy,Pr)FeB magnets can retain their coercivity at around 200°C like in HEV/EV motors and wind turbines. It is also necessary to reduce the total demand for Dy by developing low-Dy RE (NdFeB or PrFeB) magnets and a program to recycle RE magnets. During development of the $Pr_{15}Fe_{bal}Co_8B_7Nb_{0,05}Ga_{0,25}$ (no Dy) magnet, the TEM studies showed an amorphous region with a 5 nm grain boundary, as shown in Figure 44.

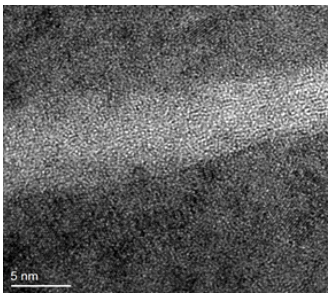


Figure 44. TEM image of $Pr_{15}Fe_{bal}Co_8B_7Nb_{0,05}Ga_{0,25}$ (Dy free) magnet.

### Ag-In-Cd control plates

A program to develop new control elements for the IEA-R1 Research Reactor at IPEN was undertaken. The first stage of this program was to make an Ag-In-Cd ingot (Figure 45A). This ingot was forged and rolled to prepare rectangular plates, to be inserted and sealed in stainless steel envelopes using a laser welding process (Figure 45B). Two such envelopes would be part of a control element.

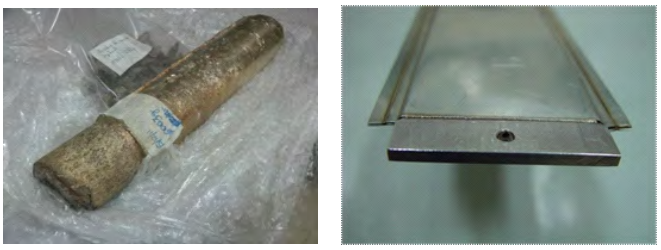


Figure 45. (A) Ag-In-Cd ingot for Control Plates; (B) Laser welded stainless steel envelope to house Ag-In-Cd and for use as IEA-R1 control element.

### Hydrogen induced degradation

A detailed study of hydrogen induced degradation of zircaloy-4 fuel tubes used in PWR reactors was carried out. The study involved determination of the threshold stress intensity factor KIH at 250°C and 227°C of zircaloy-4 tubes charged with 125 ppm of hydrogen. This study carried out in CCTM was part of a global round-robin test involving 10 countries with PWR reactors and coordinated by the IAEA.

### The production of metallic zirconium sponge by chlorination of its oxide and by magnesothermic process

Metallic zirconium is a material of high technological importance due to its high strength and corrosion resistance. Moreover, its relatively low thermal neutron cross section makes its alloys suitable to clad nuclear reactor fuel. Production of metallic zirconium sponge is under development at IPEN and this includes the following steps: a) pelletizing of zirconium oxide powder, carbon and a binder; b) chlorination of zirconium oxide and carbon pellets using chlorine gas at higher temperatures; c) purification of zirconium tetrachloride by selective sublimation; d) thermal reduction of zirconium tetrachloride with magnesium, and e) separation of metallic zirconium sponge from the slag by distillation.

A mixture of zirconium dioxide, carbon and binder powders was pelletized and green pellets between 1.0 cm and 1.5 cm in diameter

(Figure 46) were obtained. The pellets were calcined at 600°C in an inert gas atmosphere. Chlorination of the pellets was carried out in muffle furnace at temperatures of 800 to 900°C. Difference in the volatilization temperature of the chlorides permits condensation of zirconium tetrachloride in the primary condensers, maintained at 150 to 180°C (Figure 47).

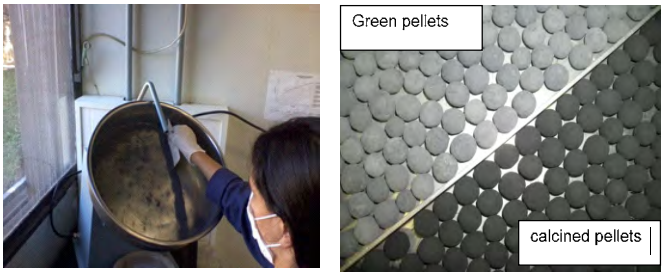


Figure 46. Pelletizing process of a mixture of zirconium dioxide, carbon and binder powders.

Figure 47. Chlorination process of zirconium oxide.

The impure $ZrCl_4$ from the chlorinator may contain Fe, Cr, Al and others impurities that are removed in a subliming furnace. The Figure 48 shows pure $ZrCl_4$. The reduction process of $ZrCl_4$, namely, contact of its vapors with a molten reducing agent, magnesium. When a reduction run is to be made, the magnesium metal and the zirconium tetrachloride are placed in the containers, and these are put into the reduction furnace (Figure 49).

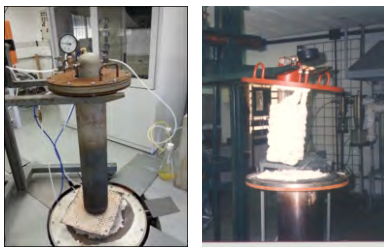


Figure 48. Container for purification of $ZrCl_4$ (A) and purified zirconium tetrachloride (B).

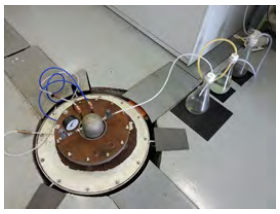

Figure 49. Unit for experimental reduction of $ZrCl_4$.

The product of the reduction operation is a mixture of zirconium metal, magnesium chloride, and magnesium metal. The experiments that were carried out showed that it is feasible to remove the magnesium chloride by vacuum distillation. Figure 50 shows zirconium sponge obtained from by distillation.

Starting with commercial grade and there after nuclear grade raw materials, high purity ductile metallic zirconium was obtained (Figure 51).

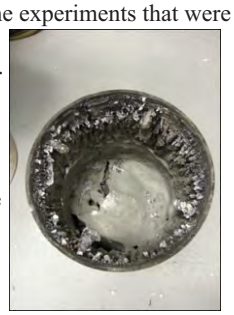

Figure 50. Zirconium sponge obtained from by distillation.


Figure 51. Zirconium sponge.

## Zircaloy 4 chips recycling and consolidation

A very large amount of Ziconium alloy scrap is generated during the machining operations, necessary to produce the nuclear fuel cladding parts (tubes, end plugs, spacer grids, etc). The melting of zirconium and its alloys requires very specific operational conditions - high dynamic vacuum, high temperature power source and rapid solidification. The process technology to attain these conditions is the Vacuum Arc Remelt process and this is accepted by the nuclear industry.

As a part of a joint project coordinated by FINEP, the Melting Laboratory at CCTM/IPEN was chosen to develop the technology to consolidate and recycle Zircalloy 4 scrap generated at INB (Indústrias Nucleares do Brasil). Typically, VAR furnaces melt high density electrodes (solid density) and the main problem regarding consolidation of Zircalloy-4 scrap is melting of pressed low density electrodes (actual solid about 20%). To achieve this goal a special device had to be designed and constructed to specifically melt low density electrodes with the laboratorial scale VAR furnace at CCTM.

In other words, the original VAR process had to be modified. Preliminary experiments with steel scrap provided ingots for further melting to form larger ingots. Otherwise, Zircalloy wetting characteristics at high temperature, above the melting temperature of 1900 °C, imposes further development of the process. This development is being carried out and will be evaluated during 2014. Further tasks were assigned to the project. These include retrofitting of the VAR furnace with new electro-electronic commands, automation, and a high speed data acquisition capability for basic electric arc research, as shown in Figure 52.


Figure 52. (A) VAR furnace; (B) command "box"; (C) retroffited power source.

## Mechanical properties of zirconium based alloys

Zirconium-based alloys are among the most widely used nuclear material, particularly zircaloy-2 and zircaloy-4. These are chosen as cladding materials of fuels used in LWR type nuclear reactors, due mainly to their excellent mechanical properties and corrosion resistance. The precipitates present in their microstructure play an important role in terms of the properties of these alloys. Initially we carried out a critical review of neutron irradiation effects on microstructural stability of the zircaloys (2 and 4). Analysis of zircaloy components exposed to typical neutron fluence, as a function of time, and under typical operating conditions affects the stability of the precipitates (Figure 53). This could produce changes in mechanical properties of these alloys, which is of paramount importance for intended applications of this alloy.

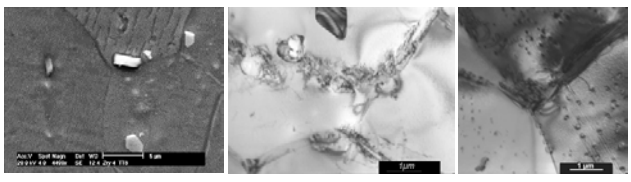

Figure 53. Second phase particles in zircaloy-4.

Zirconium alloys are used in nuclear reactor cores and are exposed to high-temperature water. During service, hydrogen generated in corrosion processes is readily absorbed by these materials. When the hydrogen concentration exceeds its solubility limit it precipitates as zirconium hydride ($ZrH_2$) in the form of platelets or needles (Figure 54). Zirconium alloy components can fail due to hydride cracking if they contain large flaws and are highly stressed. The alloys are susceptible to a crack initiation and propagation mechanism termed delayed hydride cracking (DHC). This line of research investigates the fracture mechanics of the hydrided zirconium alloys (Figure 55). The presence of brittle hydrides, with a low fracture toughness, results in severe loss in ductility and toughness when platelets are oriented parallel to the applied stress. In plate or tube, hydrides tend to form perpendicular to the thickness direction due to the texture introduced during manufacture. Hydrides oriented in this manner do not generally cause structure related problems because the applied stresses in the through-thickness direction are very low. However, the high mobility of hydrogen in a zirconium lattice causes redistribution of hydrides normal to the applied stress direction, which can result in localized embrittlement. When a platelet reaches a critical length it ruptures. If the tensile stress is sufficiently great, crack initiation starts at some of these hydrides. Crack propagation occurs by when this process keeps repeating at the crack tip. Delayed hydride cracking can degrade the structural integrity of zirconium alloys during reactor service.

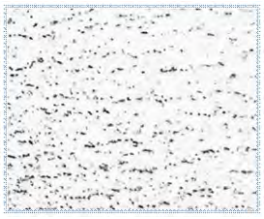

Figure 54. Hydrided microstructure of Zircaloy-4 cladding tube material.


Figure 55. Typical optical fractograph of Zircaloy-4 specimen subject to DHC conditions.

## Laboratory for analysis of irradiated materials

CCTM technical staff is involved in the preliminary conception and basic design of the Laboratory for Analysis of Irradiated Materials (LAMI). LAMI is a hot laboratory that is being designed to characterize irradiated fuel and structural materials and will be one of the main installations of the Brazilian Multipurpose Reactor (RMB). The main objectives of LAMI are: (i) to contribute, through theoretical and experimental investigations, to the development of know-how in materials science that will help predict the evolution of physical and mechanical properties of materials under service conditions (irradiation, thermomechanical solicitation, influence of the environment, etc.); (ii) to characterize the properties of materials used in the nuclear industry in order to determine their performance and to predict their life expectancy; (iii) to establish, maintain and make use of the generated database to provide expertise regarding industrial components, in particular to investigate deformation or fracture mechanisms. The materials to be tested can be irradiated or not, and originate from surveillance programs, experimental neutron irradiations or simulated irradiation with charged particles.

LAMI will have 10 shielded hot cells. The LAMI building will also have an area assigned for micro and nanostructured materials analysis. Mechanical property testing of irradiated materials will be carried out at LAMI to help comprehend damage processes and the test data will be incorporated in a data bank to maximize its use. Materials to be tested will be alloys used in industrial and experimental reactors and will include pressure vessel steels, stainless steels for internal components, austenitic-ferritic steels, zirconium alloys and aluminum alloys.

## Materials for hydrogen storage

The intermetallic compound TiFe is well known for its properties as a hydrogen storage material. A new route to produce nanostructured TiFe by high-energy ball milling was developed (Figure 56). This route was effective in preventing adhesion of particles to the grinding balls and to the walls of the vial during milling. It also provided better yields. Mixtures of $TiH_2$ (instead of Ti) and Fe powders were dry-milled in a planetary mill and then heated under dynamic high-vacuum for the synthesis reaction at 650$^0$C. Hydrogen intake can take place during the cooling stage (Figure 57), preventing tedious activation treatments often performed to achieve first time hydriding of TiFe.

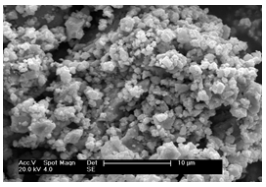

Figure 56. Hydrided microstructure of Zircaloy-4 cladding tube material.

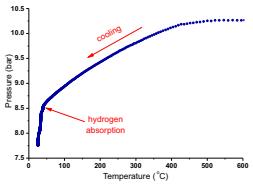


Figure 57. Hydrogen absorption curve of TiFe during cooling.

The aim of this line of research is to develop user friendly software for integrated synthesis and interactive visualization of crystals and microstructural 3D models, mainly for use as an educational tool. Students, teachers and researchers will be provided with powerful tools to aid in learning, teaching and research activities, covering basic and advanced Materials Science and Engineering topics. Screenshots presented below exemplify some features of a forthcoming open source platform that have already been implemented. Figure 58 displays a model of a simple cubic crystal structure. Figure 59 shows the microstructure of a single-phase polycrystalline material.

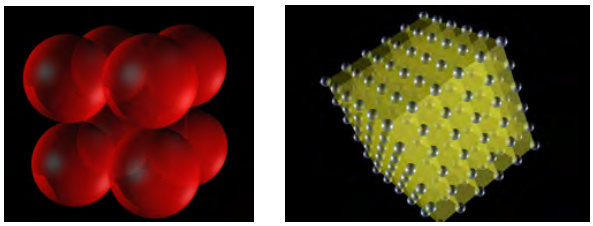


Figure 58. Simple cubic structure. A: Unit cell; B: Cristal view.

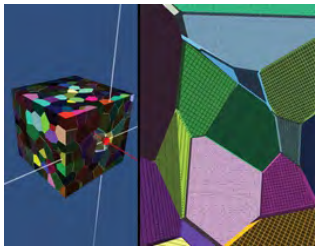

Figure 59. Microstructure modeling in 3D (left) and 2D (right).

## X-ray diffraction analysis

### Residual stress evaluation

*Aluminum based alloys:* Shot peening is a surface cold work process and is used to increase fatigue life, which can be evaluated from measurement of residual stresses. The peen forming process is a variant of the shot peening process, where a curvature in the plate is obtained by compression of the grains near the surface. The influence of parameters such as: pressure of shot, shot ball size and thickness of aluminum 7050 samples with respect to residual stress profile and resulting arc height was studied. The results show that the formation of the curvature arc height is proportional to the shot peening pressure, to the sphere size and inversely proportional to the thickness of the sample, and that the stress concentration factor is larger for samples shot peened with small balls.

*Strain gages - wheels evaluation:* Many engineering specifications, manufacturing, inspection and quality control procedures require that the residual stress of specific components be evaluated. This is becoming as commonplace as determination of mechanical properties. Residual stresses in metallic components arise as a result of manufacturing processes (casting, heat treatment, machining and mechanical forming) to achieve the desired shape of the component. This study had as its objective extension of knowledge regarding residual stress phenomena in wheels often determined by strain gage extensometry and to make available this information to improve the database for finite element analysis (FEA). Specifically, this work was undertaken to evaluate cast $AlSi_7$ alloy wheels for use in passengers cars. The residual stress values obtained from the experimental tests (consisting of drilling with rosette type strain gages and x-ray diffraction analysis at critical regions (the spokes), after correction calculations for the effect of plasticity) gave results that demonstrated the existence of convergence within the same order of magnitude with values calculated using FEA simulation software, i.e., around - 145 MPa to 80 MPa. The relevance of this study and research on residual stresses meets the expectations of safety improvements in the automobile wheel industry.

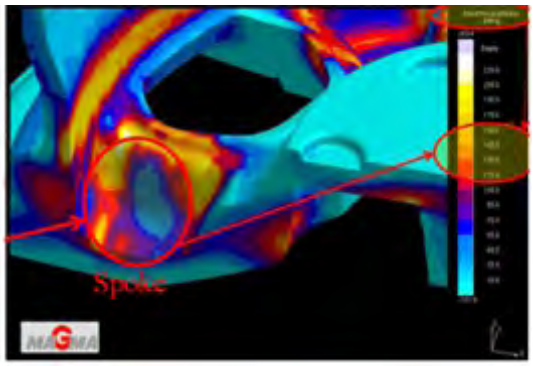


Figure 60. FEA simulation of the residual stresses calculated for an aluminum silicon alloy wheel at the spoke region.

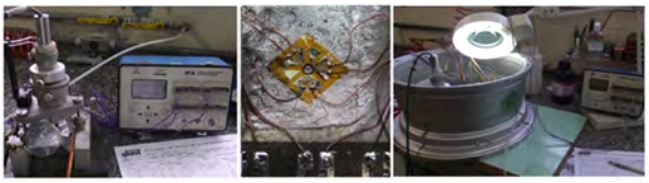

Figure 61. Sequence of the experimental strain gage with blind hole method.

*Cylinder liners evaluation:* In this project, it was possible to prove from the fatigue test that the endurance of the cylinder liner can be improved by the compressive residual stress induced by cold rolling of the filet radii. Using the Design of Experiments (DOE) methodology, an experiment was created to study the individual contribution of each parameter of the cold rolling process (force, time and speed) on the increase in compressive residual stress. The x-ray diffraction technique enabled the measurement of the residual stress of all cylinder liners used in the DOE experiment. Statistical techniques like Analyze of Variance (ANOVA), Pareto chart and the Anderson-Darling normality test were applied to the set of results obtained from the x-ray diffraction measurements, making it possible to determine that force is the parameter which has the highest influence on increasing the compressed residual stress in the filet radii. The effectiveness test of the residual stress measurement by x-ray diffraction, proved that this methodology has adequate resolution to detect production mismatch, making it a better substitute for the fatigue test, which is nowadays used to inspect the cylinder liners.

*Automotive springs evaluation:* Regarding automotive springs, the shot peening process has become an essential step in manufacturing. In the case of leaf springs, however, a systematic investigation of the effect of shot peening on fatigue life is still required. Through analysis of residual stresses from x-ray diffraction studies and fatigue tests on a series of samples that were subject to ten different peening schedules, it was possible to demonstrate the role of shot peening during manufacture of leaf springs for vehicles in improving properties. Among the investigated processes, the use of 0.8 mm diameter cast steel shot followed by a second peening with 0.3 mm diameter cast steel shot lead to optimal performance, regarding fatigue life.

### Crystallographic texture

A comparative microstructural study has been carried out of AA4006 alloy strips produced by two industrial casting processes: twin roll caster (TRC) and direct chill (DC). X-ray diffraction was used for texture characterization. Significant differences in morphologies and in the distribution of grains and intermetallic particles were observed. The crystallographic texture throughout the thickness of these strips was determined and the results revealed significant differences. Texture analysis was carried out using the x-ray diffraction technique. The twin roll caster (TRC) sheet showed a typical shear texture near the surface, while internally, the β-fiber was observed.

Medium carbon steels are mostly used for simple applications; nevertheless new applications have been developed for which good sheet formability is required. This class of steels has low formability.

is required. This class of steels has low formability. A medium carbon hot rolled SAE 1050 steel was selected for this study. It was cold rolled with reductions in the 7-80% range. Samples were used to determine the cold work hardening curve. For samples with 50 and 80% thickness reduction, an annealing heat treatment was given to achieve recrystallization. The 50% cold rolled and recrystallized material was studied in terms of sheet metal formability and texture evolution during the actual stamping of a steel.

**Crystallography applied to materials science**

The Laboratory of Crystallography Applied to Materials Science - CristalMat - was created in 2012 to study, develop and apply techniques of crystallography in the study and development of materials. The group is composed of researchers from the Materials Science and Technology Centre and collaborators from other groups in IPEN, external collaborators from national and foreign research institutions, postdoctoral fellows, doctoral, master's and undergraduate students.

The main objectives of the group are the application of crystallographic techniques in the study of crystal structure and microstructure of materials with the purpose of optimization of properties and processes, development of new materials or new applications of these materials. These techniques include, x-rays, neutron and synchrotron radiation diffraction, x-ray and neutron absorption as well as scattering and x-ray fluorescence.

The infrastructure of CristalMat is made up of equipment acquired in a joint project with the Brazilian Nuclear Industries - INB, for technology development for the production of nuclear grade metallic zirconium and its alloys for nuclear applications. The group also obtained support from projects financed by other Brazilian agencies.

The CristalMat group interacts with research groups in Brazil and abroad, mainly to develop projects, conduct scientific research and also for the exchange of graduate students and scientists. The group also interacts with public and private companies, providing analysis and project development services. Researchers from the CristalMat Group offer courses within the IPEN/USP Nuclear Technology Graduate Program.

The CristalMat Laboratory has the following equipment and facilities: Rigaku ULTIMA IV x-ray diffractometer with Cross Beam Optics and other attachments (Figure 62); Cu and Cr radiation sources; Rigaku PRIMINI wavelength dispersive x-ray fluorescence spectrometer (Figure 63), zero background sample holders; certified standard reference materials for powder diffraction; crystallographic and powder diffraction databases; an extensive collection of free, academic and commercial crystallographic software, including some developed by the group. The group has also access to some other equipment and facilities owned by other collaborating institutions, like the synchrotron laboratories of Brazil and Spain.


Figure 62. Rigaku ULTIMA IV x-ray diffractometer.

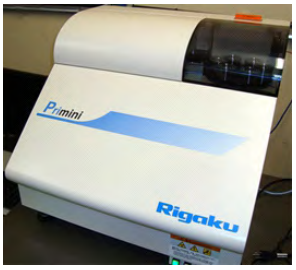


Figure 63. Rigaku PRIMINI x-ray fluorescence spectrometer.

The group works, among others, in the following areas of research: applied crystallography; materials characterization; x-ray, synchrotron and neutron diffraction; x-ray fluorescence spectroscopy; microstructural analysis of materials; development of standard materials for powder diffraction; x-ray line profile analysis; Rietveld method; zirconium and its alloys; processes for reusing of Zircaloy scrap by arc-remelting and powder metallurgy; metals and advanced alloys; advanced ceramics; nuclear fuel; bioceramics and biomaterials; residual stresses in welding of duplex stainless steel; high Tc superconductors, electrical and magnetic ceramics; corrosion products; nanoferrites; rare earth magnets; nanostructured materials; materials for fuel cells; characterization of advanced cements used for radioactive waste immobilization and oil industry; instrumentation for x-ray diffraction and absorption in-situ measurements at high pressures etc.

The technological development of this group include: (a) the production high quality “Standard Reference Materials for Powder Diffraction” can be cited and these are being used in more than twenty universities in Brazil, South-America and Europe, and at research institutes like the Brazilian Synchrotron Light Laboratory - LNLS and ALBA Synchrotron Facility (Spain); (b) the development of processes for reusing of nuclear grade Zircaloy scrap by arc-remelting and powder metallurgy methods.

### Potential applications for the use of rare earth complexes and nanoparticles as luminescent biolabels

The ever growing interest in rare earth coordination compounds and materials with optical properties stems from applications in multidisciplinary fields such as nanosensors, materials for telecommunications, lighting devices, and luminescent probes for bioanalyses and live cell imaging and sensing. Most of these applications use the unique ability of the rare earth ions to emit well-defined narrow bands in different spectral ranges, from visible to near-infrared. Due to the low absorption cross-section of the f-f transitions, efficient population of the excited 4f states has to rely on energy transfer from the surroundings of the metal ion (antenna effect or luminescence sensitization). Another point desirable is the use of $RE^{3+}$ ions with emission in the near-infrared (NIR) region reducing the interference from biological materials in the analyses.

At this time we have gave attention and report here the preparation and characterization of rare earth coordination compounds and nanoparticles based on rare earth ions. $RE^{3+}$ β-diketonate complexes with macrocyclic, phosphine oxide and carboxylate ligands, has been synthesized and characterized and are being used to mark hemoglobin S (sickle cells) *Leishmania* (tropical desease) and PSA (Prostate-specific antigen that is a protein produced by cells of the prostate gland. The PSA test measures the level of PSA in the blood). $RE^{3+}$ β-diketonate complexes of tetracycline, piroxican and fluoxetine are been developed as urine sensor. Several nanoparticles based on $Nd^{3+}$, $Eu^{3+}$ and $Tb^{3+}$ ions doped into the $Y_2O_3$ matrix, are also being synthesized and evaluated for labeling anti-oxLDL (anti-oxidized low density lipoproteins), one of the principal causes of cardiovascular diseases and responsible for around 30% of deaths world-wide. Information about structure and average grain size of these nanoparticles were obtained by x-ray diffraction (XRD), transmission electron micrograph (TEM) and infrared absorption spectroscopy. The thermal properties and luminescence phenomena are also evaluated.

### Synthesis and characterization of $SnO_2$@ $TiO_2$ nanoparticles doped with nlanthanide for biological labeling

Fluoroimmunoassay is an ultrasensitive technique for investigation of enzymes, antibodies, cells, hormones and others. The demand for highly sensitive systems brought the nanomaterials for biomedical and biotechnological field. Semiconductor nanocrystals (quantum dots) doped with lanthanide ions, when functionalized with biomolecules, can be used as luminescent biomarkers. Aiming this application, we have been synthesized and characterized nanoparticles of titanium and tin mixed oxide doped with europium, terbium and neodymium. The synthesis was made by the co-precipitation method and characterized by SEM, IR, XRD, TGA and luminescence spectroscopy. These particles were functionalized by silica using two different methods, the microwave method and Stöber method to facilitate the conjugation with biological entities.

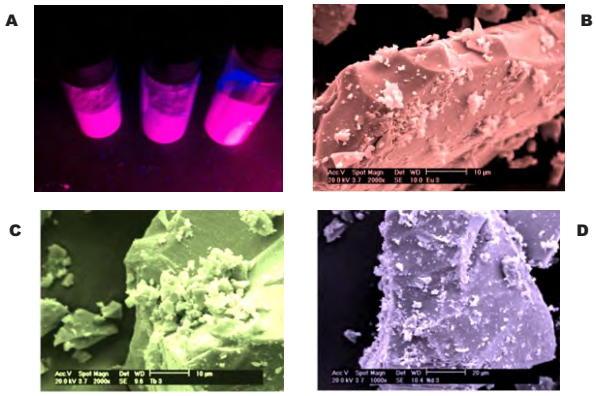


Figure 64. Nanoparticles of $SnO_2/TiO_2:Eu^{3+}$ (A), Mev $SnO_2/TiO_2:Eu^{3+}$ (B), Mev $SnO_2/TiO_2:Tb^{3+}$ (C) and Mev $SnO_2/TiO_2:Nd^{3+}$ (D).

### Synthesis and characterization of $TR_2(MoO_4)_3$@ $SiO_2$ nanoparticles doped with $Eu^{3+}$, $Tb^{3+}$ and $Nd^{3+}$ for biological labeling

The interest in using rare earths to investigate the properties and functions of biochemical systems as well as to determinate biological substances has increased in several fields, including biomarkers in immunology (fluoroimmunoassays). Nowadays the use of lanthanides in the diagnosis of various diseases have become more important through the development of commercial diagnostic kits. As main feature, these rare earths can show a long lifetime, photostability and emission bands of atomic like behavior and well defined, in the visible region, demonstrating unique advantages when compared to other luminescent species. The present research synthesize rare earth molybdates by the co-precipitation method as well as characterize these materials by X-ray diffraction, near infrared spectroscopy, thermogravimetric analysis, scanning electronic microscopy, transmission electronic microscopy and luminescent studies. This research focuses, three different studies as followed: the influence of the vortex speed variation during co-precipitation in the structure of the final product, morphology and luminescence properties; the influence of the annealing temperature also in the structure, morphology and luminescence properties; and the influence of concentration of the doping in the luminescence properties. Another important step of this research is the functionalization of nanoparticles using an organosilane (APTES) to coat and establish points for binding the particles to biological species. It was proved that this process was very efficient by the characterization results and the silica incorporation was well succeeded. Specific prostatic cancer (PSA) was then linked to the functionalized nanoparticles to diagnostic prostatic cancer by fluoroimmunoassay and levels for detection were established.

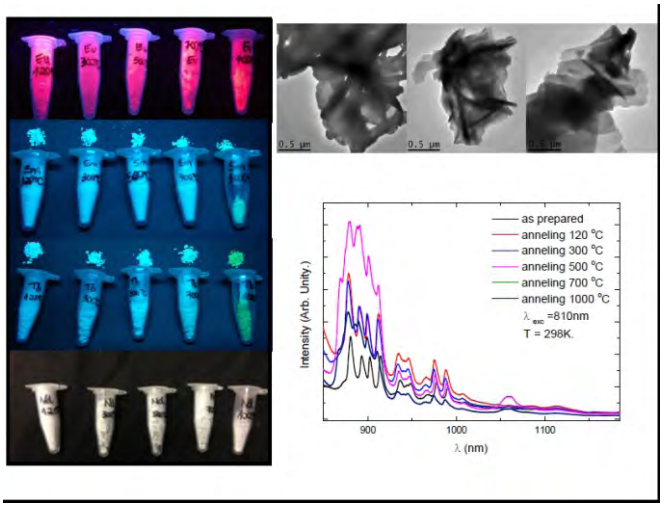


Figure 65. Ilustration of $TR_2(MoO_4)_3$ under excitation of UV lamp, TEM of the $Nd_2(MoO_4)_3$ and $TR_2(MoO_4)_3$@Si Microwave and $TR_2(MoO_4)_3$@Si Stöber and emission spectra of the $Nd_2(MoO_4)_3$.

### Europium βetha-diketonate complexes with tetra cycline(TC), fluoxetine(FL) and piroxican (PX)

Luminescent materials containing trivalent rare earth ($RE^{3+}$) complexes with β-diketonate ligands have been intensively studied in recent years. The $RE^{3+}$ compounds present characteristic narrow emission bands in the UV-Vis region, large Stokes shift and the antenna effect that enhance the overall quantum efficiency, As a result, these complexes have found wide applications as luminescent markers, photoluminescent sensors, electroluminescent devices, and multicolor display. In the field of biomarker these compounds linked with biological parts.

At this time it was synthesized new complexes of europium β-diketonate with tetracycline,piroxican and fluoxetine as ligand. IR spectra of the Eu(III) complexes show two strong absorption bands at ~1597 and ~1566 $cm^{-1}$ attributed to $\nu_s$(C=O) and $\nu_{as}$(C=O) vibrational

stretching modes, suggesting that the β-diketonate ligand acts as chelate ligand. SEM image showed particles rounded with grain size lower than 10 nm. The emission spectrum of europium complexes, in the solid state, recorded in the range of 420 to 720 nm at liquid nitrogen temperature, under excitation at β-diketonate transitions (~350 nm) is shown in Fig. 66. This emission spectrum exhibits characteristic narrow emission bands that are assigned to the $4f^6$-$4f^6$ transitions of Eu(III) ion, attributed to the emitting $^5D0$ level to the $^7FJ$ (J = 0, 1, 2, or 4) levels, where the most intense corresponds to $^5D0^7F_2$ transition taking place around 613 nm. An important feature to be observed is the nonexistence of broaden bands arising from the β-diketonate centered transitions, indicating that intramolecular energy transfer from the β-diketonate ligands to the Eu(III) ion is operative.

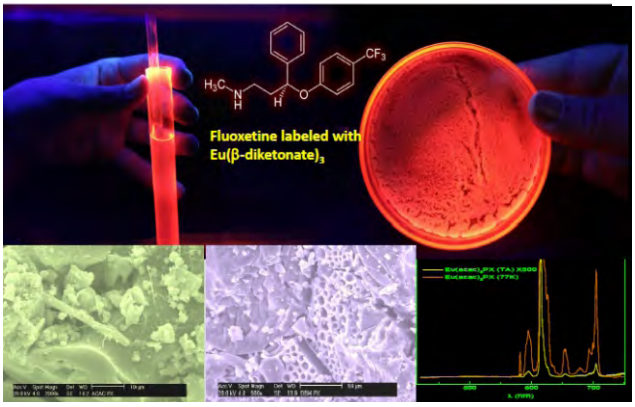


Figure 66. Luminescent biomarkers for chemicals detection in biologic fluids. UP Fluoxetine europium compound undet UV excitation, Down SEM image of compounds and emission spectra of Eu-β-diketonate-piroxican compound.

## Luminescent material based lanthanide complexes incorporated into modified silica particles for biological applications

Amino-functionalized luminescent silica particles were investigated for use in immunoassays. The particles were prepared by the *Stöber method* where the Lanthanide complexes (β-diketonates, or carboxylate) were incorporated into silica particles during the hydrolysis and condensation of TEOS: tetraethylorthosilicate (Fig 67). Then, the amino groups were introduced in the particle surface using APTES: 3-aminopropyltriethoxisilane. The resulting particles were characterized by scanning electron microscopy (SEM), X-ray diffraction (XRD) and photoluminescence spectroscopy. In order to demonstrate the viability of the use of luminescent particles as optical markers, an enzyme-substrate reaction was performed using HRP: horseradish peroxidase. It was possible to verify the binding of HRP-protein) and anti- antibody-luminescent silica particles through the evaluation of the presence of HRP. The bioassay data open a broad field for the development of protein-tagged luminescent particles for use in biomedical sciences.

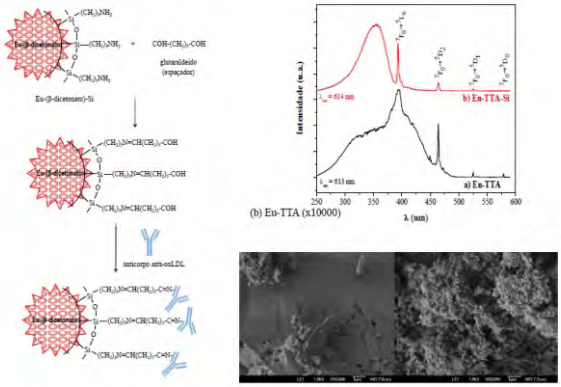


Figure 67. Schematic conjugation of luminescent nanoparticle with antibody(a), excitation spectra of Eu-TTA-Si and Eu-TTA and SEM of the complex and the particle.

## Development of nanobiomarkers for use in sickle cell anemia

Luminescent materials, such as the rare earth's complex, can be used as markers in cytology and immunology, being also used as luminescent biomarkers, once the development of these nanomaterials create new possibilities to many fields, particularly in diagnostic medicine. Besides, it establishes one kind of fluorescent probes, for which there are no equivalent organic molecules. Due to its potential in market's application, the objective of this work was to develop luminescent materials, allowing the use of these supermolecules of lanthanides as markers for the detection of Sickle Cell Disease (HbS). Six luminescent markers were developed based on rare earth compounds. The main methodology used for the detection of HbS was fluoroimunoassay, which is already used in investigation of enzymes, antibodies, cells, hormones, and so on. During this work, absorption's spectrum in the infrared by Fourier's Transform (FTIR) was also used to detect the HbS.

The studied methods were applied for the diagnosis of this disease, which has genetic origin, very typical of the hemoglobin-pathology group and considered to be a public health problem in Brazil (ANVISA). When early diagnosed, Sickle Cell Disease (SCD) has a significant decrease in morbidity and mortality. Comparing the obtained results to the already known methodologies, it was possible to conclude that they are viable methods to detect HbS. Besides, when totally developed, these methods will contribute to the production of Sickle Cell Anemia's diagnostic, and they will have impact in São Paulo state's public measures, as well as in Brazil's ones.

We are extending our tools to validate a safe, sensitive and inexpensive methodology. Therefore we are using the Maldi-Toff method in order to have a better understanding of the peptide profile on the target of biological materials. We will also make a database of most peptides present in the sickle cell disease and do the biomarking of HbS with $^{131}$Iodine for comparative analysis of these methods.

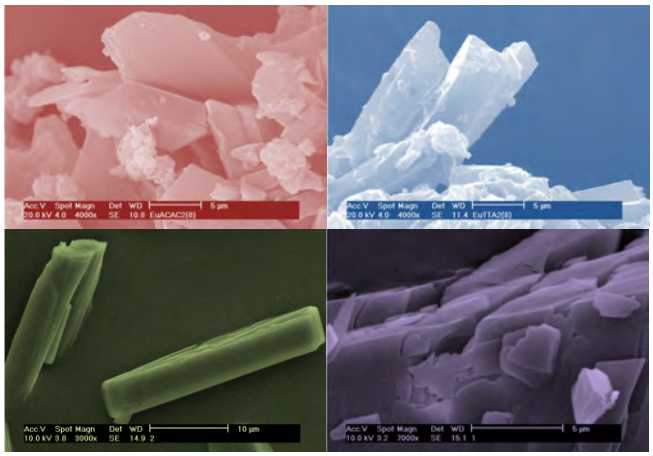

Figure 68. SEM of the Europium and terbium supermolecules.

## Luminescent polymeric nanoparticles (LUMPNP) for biological labeling

A major difficulty in biomarker process is related to the solubility of the nanoparticles in the biological media. This fact limits the process of bioconjugation and consequently the signaling. Beside of these facts it has been working with polymer (PMMA, PHB, Chitosan) markers that are easier to be functionalized with biocompatible chemical group , which probably facilitate the reactions with biological entities. In this context two methods of synthesis for implementation of the project were chosen: the first method synthesizes the nanoparticle by cryogenics technique and the second method is the microemulsion technology. Figure 69 shows the SEMs images of these particles and it can be seen that the particles are more dispersible than the particles used previously. It can also be noted that the polymer nanoparticles

incorporating the complexes [TR (β-diketone)$_3$ (Ligand)$_x$] showed emission quantum efficiencies close to 100%. The PMMA polymer nanoparticles doped with 0.5 to 5% by weight of the europium complex were functionalized with a diamine to act as a spacer in bio conjugation. (Fig 70)

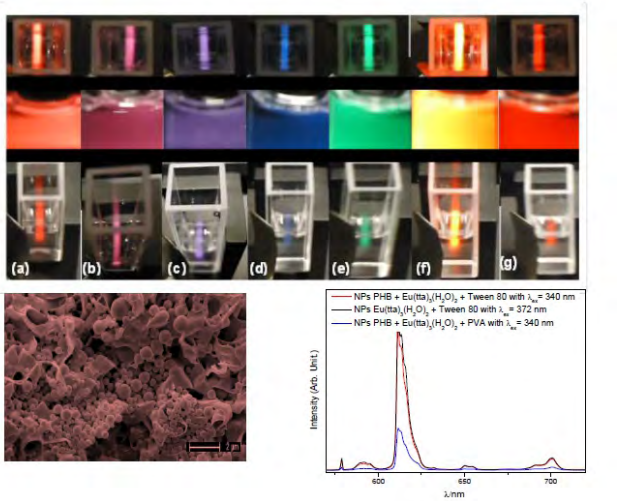


Figure 69. Luminescent polymeric nanoparticles (NPPLUM) for biological labeling-nanoemulsion. Nanoparticles under utraviolet irradiation (a) PHB + [Eu(tta)$_3$(H$_2$O)$_2$]; (b) PHB + [Eu(acac)$_3$(H$_2$O)$_2$]; (c) PHB + [Sm(tta)$_3$(H$_2$O)$_2$]; (d) PHB + [Sm(acac)$_3$(H$_2$O)$_2$]; (e) PHB + [Tb(acac)$_3$(H$_2$O)$_2$]; (f) [Eu(tta)$_3$(H$_2$O)$_2$]; (g) PHB + [Eu(tta)$_3$(H$_2$O)$_2$] + PVA (up) and SEM and emission spectra of the PHB-Eu nanoparticles.

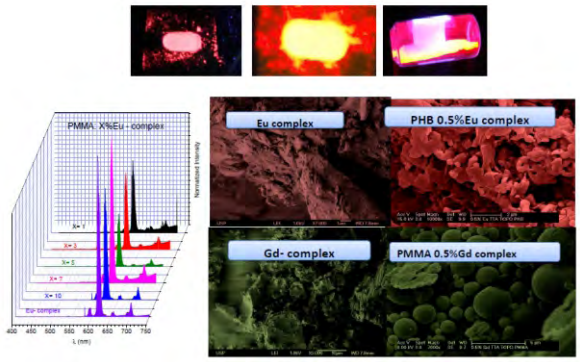


Figure 70. Luminescent polymeric nanoparticles (LUMPNP) for biological labeling-cryogenics a) Europium nanoparticles under UV exitation; b) Emission spectra of NPPLUM; c) SEM of precussor and NPPLUM.

## Luminescence-tuneable multicolour PMMA films doped with lanthanide β-diketonate complexes

Interest in luminescent materials containing trivalent lanthanide ions ($Ln^{3+}$) as emitting centers has grown significantly in recent years. However, the $Ln^{3+}$-complexes generally present low thermal stability, limited photostability and poor mechanical properties. Another parallel challenge is that most of these compounds are usually achieved as hydrates, consequently the luminescence intensity is suppressed due to the activation of non-radiative channels. In order to overcome simultaneously these deficiencies and improve the characteristics of light emission (*e.g.* quantum yield, lifetimes), $Ln^{3+}$-complexes have been incorporated into organic polymers, liquid crystals and sol-gel derived organic-inorganic hybrids. Polymers offer several advantages for the development of materials, such as: flexibility, versatility, optical quality and moderate processing conditions. By incorporating luminescent $Ln^{3+}$-complexes within the polymer matrix, the resulting product represents not only the sum of individual contributions of both organic and inorganic phases, but also novel properties for a new class of materials.

In the present work, diaquatris(thenoyltrifluoroacetonate)-europium(III), [Eu(tta)$_3$(H$_2$O)$_2$], di triphenylphosphine oxide (thenoyltrifluoroacetonate)-europium(III), [Eu(tta)$_3$(TPPO)$_2$], triaquatris(acetyl-acetonate)Terbium(III), [Tb(acac)$_3$(H$_2$O)$_3$] and triphenylphosphine oxide (acetyl-acetonate)Terbium(III), [Tb(acac)$_3$(TPPO)$_2$], [Tb(acac)$_3$(n-picNO)$_2$], complexes were co-doped into the PMMA and PHB polymer in order to obtain multicolor light-emitting devices due to their strong luminescence and relatively simple and inexpensive preparations.

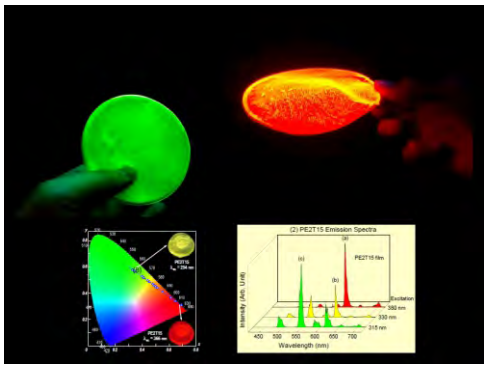


Figure 71. PMMA: x%[Tb(acac)$_3$(TPPO)$_2$] and [Eu(tta)$_3$(TPPO)$_2$], irradiated at UV light CIE chromaticity diagram showing the x,y emission color coordinates for PMMA:Eu(tta)$_3$:Tb(acac)$_3$ films irradiated at different wavelengths (B) and emission spectra with excitation at: 380, 330 and 515 nm (C).

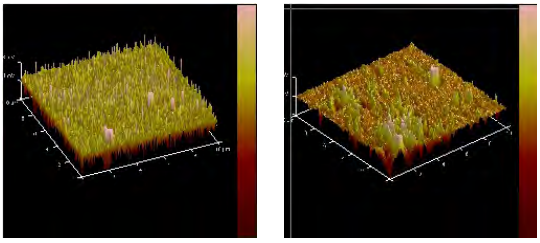

Figure 72. AFM of PMMA films undoped and doped with Tb(acac)$_3$(TPPO)$_2$.

## Bifunctional magnetic and luminescente nanoparticles for diagnostic

The design of bifunctional luminescent magnetic nanomaterials containing $MFe_2O_4$ (where M=Fe and Mn) doped with rare earth and functionalized with rare earth ions inclusion complexes of calixarene and phosphine oxide and β-diketonate ligands or chitosan natural polymer have been investigated. These novel $MFe_2O_4$ @Ln complexes) luminescent magnetic nanomaterials present very interesting superparamagnetic and photonic properties. The magnetic properties were explored at 5 and 300K temperature and come to know that the extent of coating and crystallinity affect the saturation magnetization values of nanoparticles. Although ferrite is strong luminescence quencher, the coating of the $MFe_2O_4$ nanoparticles has overcome this difficulty. The intramolecular energy transfer in the nanomaterials from the $T_1$ excited triplet states of TTA and ACAC ligands to the $^5D_0(Eu^{3+})$ and $^5D_4(Tb^{3+})$ emitting levels have been determined. In addition to the superparamagnetic behavior, these nanophosphors may be act as emitting layer of red and green light converting molecular devices (LCMDs).

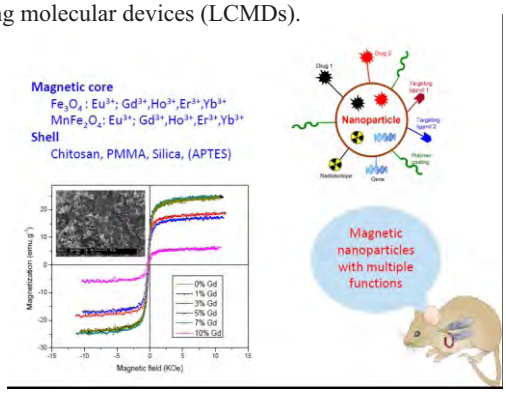


Figure 73. Magnetization curve of manganese ferrite doped with gadolinium inserte figure SEM of this material.

## Materials for security and solar cell storage

**Thermoluminescence and synchrotron radiation studies on the persistent luminescence of $BaAl_2O_4:Eu^{2+}$, $R^{3+}$ and and $CdSiO_3$: $TR^{3+}$**

Since 1995, the research on persistent luminescence materials has increased substantially .This is due to the progress in the properties of these materials: they can emit nowadays in visible for many, up to 24+ hours, after ceasing the irradiation. Because of the long emitting time, these phosphors can be exploited commercially in emergency signs, road signalization, wall painting, watches, micro defect sensing, optoelectronics for image storage and detectors of high energy radiation. The persistent luminescence is not any more just a scientific curiosity.

According to the literature, the $BaAl_2O_4(:Eu^{2+}, R^{3+})$ materials are prepared via a solid state route, usually by heating $BaCO_3$ with $Al_2O_3$ (or their precursors) at elevated temperatures. However, low temperature routes as combustion and sol-gel syntheses are not uncommon. In the present work it was prepared $BaAl_2O_4$ materials: $Eu^{2+}$, $TR^{3+}$ through the ceramic methods and combustion, and $CdSiO^3$: $TR^{3+}$ (TR:Y, La, Ce, Pr, Nd, Sm, Eu, Gd, Tb, Dy, Ho, Er, Tm, Yb, Lu), by ceramic method , showing persistent luminescence. As usual, the combustion synthesis produces crystals with smaller size, evidently due to higher local temperature during the spontaneous explosion. Since the thermoluminescence analyses suggested the presence of one and three traps for the combustion and solid state prepared materials, respectively, the method of preparation has a significant effect on the defect structure of the materials. These materials were characterize $BaAl_2O_4$ materials:$Eu^{2+}$, $TR^{3+}$ and $CdSiO_3$:$TR_{3+}$ by absorption spectroscopy in the infrared, X-ray diffraction, scanning electron microscopy, absorption spectroscopy, X-ray structure (absorption of X-rays near the edge - XANES absorption fine structure and X-ray extended - EXAFS), electron excitation and emission spectroscopy in the regions of UV and vacuum - UV - vis and thermoluminescence. It was also investigate the photoluminescent properties of materials $BaAl_2O_4$:$Eu^{2+}$, $TR^{3+}$ and $CdSiO_3$:$TR^{3+}$ through their excitation spectra and emission and determine the values of lifetime and Band Gap and the positions of the ground states of the ions $TR^{2+/3+}$ in the Band Gap. It was developed mechanisms for the phenomenon of persistent luminescence of $Eu^{2+}$ ion doped in $BaAl_2O_4$ matrix and $TR^{3+}$ ions doped in $CdSiO_3$ matrix.

The mismatch between the band gap ($E_g$) value obtained from the synchrotron radiation excitation spectra and the DFT calculation was deduced to result from the covalent bonding in the $BaAl_2O_4$ host. The XANES spectroscopy showed a predominance of $Eu^{3+}$ which can be present as a result of the in situ conditions of persistent luminescence during the X-ray irradiation. A systematic study of the effect of other $R^{3+}$ co-dopants than $Dy^{3+}$ is needed to a better understanding of the persistent luminescence mechanism of $BaAl_2O_4$:$Eu^{2+}$, $Dy^{3+}$.

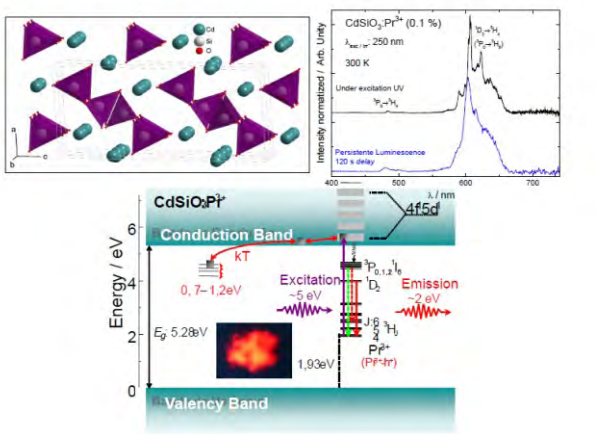


Figure 74. Structure of $CdSiO_3$:$Pr^{3+}$, emission spectra and mechanism of persistent luminescent $CdSiO_3$:$Pr^{3+}$ and inserted mechanism $CdSiO_3$:$Pr^{3+}$ under Uv irradiation.

### Research Staff

Dr. Ana Helena de Almeida Bressiani; Dr. Ana Lúcia E. Godoy; Dr. Antonio Augusto Couto; Dr. Arnaldo H. Paes de Andrade; Dr. Bakkat Ali; Dr. Carlos Alberto da Silva Queiroz; Dr. Cecilia Chaves Guedes e Silva; Dr. Chieko Yamagata; Dr. Claudio J. da Rocha; Dr. Cristiano S. Mucsi; Dr. Dolores Ribeiro R. Lazar; Dr. Eguiberto Galego; Dr. Eliana Navarro dos S. Muccillo; Dr. Emília Satoshi M. Seo; Dr. Flávia Rodrigues de O. Silva; Dr. Francisco J. C. Braga; Dr. Hidetoshi Takiishi; Dr. Isolda Costa; Dr. Ivana Conte Cosentino; Dr. Jesualdo Rossi; Dr. José Carlos Bressiani; Dr. José Roberto Martinelli; Dr. Lalgudi V. Ramanathan; Dr. Larissa Otubo; Dr. Liana Key Okada Nakamura; Dr. Luis Antonio Genova; Dr. Luis Gallego Martinez; Dr. Luzinete P. Barbosa; Dr. Maria Claudia F. C. Felinto; Dr. Marilene M. Serna; Dr. Marina Fuser Pillis; Dr. Maurício D. M. das Neves; Dr. Nelson Batista de Lima; Dr. Paula Pinheiro Paganini; Dr. Raquel de Moraes Lobo; Dr. Reginaldo Muccillo; Dr. Ricardo Mendes Leal Neto; Dr. Rodolfo Politano; Dr. Rubens Nunes de Faria Jr; Dr. Sonia Regina H. M. Castanho; Dr. Valter Ussui; Dr. Walter K. Yoshito; MSc. Edson Pereira Soares; MSc. Francisco J. Breda; MSc. Fredner Leitão; MSc. Glauson A. F. Machado; MSc. Lia Maria C. Zarpelon; MSc. Luis Carlos E. Silva; MSc. Mariano Castagnet; MSc. Oswaldo Julio Junior; MSc. Rene Ramos de Oliveira; MSc. Rui Marques de Lima; MSc. Yone V. França; Tech. Celso Vieira de Moraes; Tech. Dileusa A. S. Galissi; Tech. Marcelo A. de Oliveira; Tech. Marco Andreoli; Tech. Nildemar A. M. Ferreira; Tech. Olandir V. Correa; Tech. Pedro P. Freitas; Tech. Reinaldo A. da Costa; Tech. Thiago dos Santos Ferreira; Elizabete dos Santos; Marlene de Fátima P. Marcelino; Sandra M. Cunha.

### Graduate Students

Alexander Rodrigo Arakaki; Alexandre Amaral Sgobbi; Ana Carolina Moreira Fonseca; André Montes Rodrigues; Anelyse Arata; Arnaldo Augusto Ciquielo Borges; Bianca Alves Marcello; Bruno Ferreira Antunes da Silva; Carola G. Ágreda; Carolina Sayuri Hattori; Caroline Bernardi Machado; Caroline Ferreira Gugliotti; Cecilio A. Cunha; Chester Contatori; Clarissa Lombarde Dias; Cleiton dos Santos Mattos; Clóvis de Oliveira Junior; Daniel Nagano da Silva; Daniel Ricco Elias; Daniela Maria Cerqueira Leite; Débora Christina Salum; Débora Harumi Suzuki Hara; Diogenes Cordeiro de Souza Neto; Douglas Will Leite; E. Z. Santos; Edison Luis Gaiolo; Edney Deschauer Rejowski; Edvaldo Roberto de Souza; Elen Gonçalves dos Santos; Eleni Cristina Kairalla; Eliana Ionara de Oliveira Pesqueira; Éliner Affonso Ferreira; Eraldo Cordeiro de Barros Filho; Eurico Felix Pieretti; Everton Bonturim; Fabio Rola; Fátima Goulart; Felipe Gracio; Fernando Bardella; Francisco Carlos Ceoni; Gabriel Souza Galdino; Gisele Fabiane Costa Almeida; Guilherme Altomari Geribola; Guilherme Faria; Guilherme Luís Cordeiro; Guilherme Ramos Costa; Guilherme Scheidt; Henrique Duarte Lopes; Henry Wilson Pohling Máximo; Igor Passos dos Santos; Jacinete Lima dos Santos; José Hélio Duvaizem; Juliana Pereira de Souza; Júlio César S. Casini; Kalan B. Violin; Karolina P. S. Tonello; Klauss Engelmann; Leandro Pidoni; Lucas Campaner Alves; Luciana C. Y. Pistarini; Luis Cláudio Aranha; Luiz Alberto Tavares Pereira; Luiz de Sá M. D. Gonçalves; Mauro Machado de Oliveira; Maviael José Silva; Nancy Maeda; Narayanna Marques Ferreira Mendes; Oscar Ferreira; Pâmela Karina dos Santos Bomfim; Patrícia Brissi Santos; Patrícia Maehata; R. L. Grosso; R. M. Batista; Rafael Bruno; Railson Bolsoni Falcão; Raquel Ferreira Lucchesi Guimarães; Regiane Daniela de Campos; Renato Paulo Rezende; Roberta M. Mello; Robinson Amaro Ferreira; Rodrigo Crociati Carriel; Rodrigo U. Ichikawa; S. L. Reis; S. M. G. Carvalho; Sérgio Roberto Todesco; Silas Cardoso dos Santos; Suelanny Carvalho da Silva; T. C. Porfirio; Tadeu Noveli Cantarin; Tamiye S. Goia; Teófilo Mendes Neto; Thais da Silva Santos; Thelma Antunes Rodrigues Kovacs; Viviane Gabriel Ferreira.

### Undergraduate Students

Agatha Matos Misso; Alberto E. Sansone; Alberto Yusti; Amanda de Paula Ferreira; Amon Solano Ribeiro Lopes; André S. Barros; André Ventura Piaggio dos Santos; Beatriz de Pádua Severino; Carla Lima Aguiar; Celso Maurício Pereira de Oliveira; Edgar Djalma Campos Carneiro Dammann; Eduardo Gosik Pugliese; Eduardo José Nogueira; Edvan Almeida de Souza Filho; Fernando dos Santos Silva; Gabriel de Souza Hachisu; Gleicy de Lima Xavier; José Carlos Amaral Neto; José Felipe Ziboldi Reis; José Parra Silva; Ladislau Linheira Júnior; Leonardo Alves de Oliveira; Luan Merida de Medeiros; Luis Felipe Exner; Luiz A. Azevedo; Marcos V. Surnami; Mariana Guedes da Silva Franchi; Mayara Rafaela S. Paiva; Melissa R. Martins da Silva; Pietro Magalhães Liguori; Tatiana Martinez Moreira; Vitor Ferreira Garcia.

### Postgraduate Students

Cássio C. S. Pedroso; César dos Santos Cunha; Francisco A. Silva Junior; Helliomar Pereira Barbosa; Israel Ferreira da Costa; Ivan G. N. Silva; Jose M. Carvalho; Latifullah Khan; Tiago B. Paolini.

### Co-Workers

Dr. A. L. Horovistz; Dr. Ana Maria Segadães; Dr. Ana Valéria Santos de Lourenço; Dr. Andre Tschipstchin; Dr. Angela R. M. Castro; Dr. Angelo Fernando Padilha; Dr. Antonio Carlos da Silva; Dr. Arisbel Cerpa; Dr. Armando C. Souza; Dr. Carla C. Guimarães; Dr. Carlos de Moura Neto; Dr. Christiane Ribeiro; Dr. Claudia Akemi Kodaira Goes; Dr. Claudinei dos Santos; Dr. Claudio Geraldo Shon; Dr. D. Gouvea; Dr. D. Z. de Florio; Dr. Dachamir Hortza; Dr. Danieli Aparecida Pereira Reis; Dr. Danilo Nustafa; Dr. E. C. C. Souza; Dr. E. Caproni; Dr. E. Djurado; Dr. E. M. S. C. Tomás; Dr. Eduardo Milton Ramos Sanchez; Dr. Edval Gonçalves de Araújo; Dr. Elisabete Jorge Pessine; Dr. Elson Longo; Dr. Ercules Epaminondas de Souza Teotonio; Dr. F. de Camargo; Dr. F. M. B. Marques; Dr. Fatima Salgado; Dr. Felipe Antunes Santos; Dr. Flávio M. S. Carvalho; Dr. Francesca Deganello; Dr. Francisco J. O. Rios; Dr. Francisco Piorino Neto; Dr. Frank Ferrer Sene; Dr. G. C. C. Costa; Dr. Gilberto F. Sá; Dr. Givanildo Alves dos Santos; Dr Hermi Felinto de Brito; Dr. Hiro Goto; Dr. I. F. Machado; Dr. Idelma A. A. Terra; Dr. J. R. Carmo; Dr. Jan Vatavuk; Dr. Jorge Otubo; Dr. Jorma Hölsä; Dr. Jose Roberto Berretta; Dr. José Serafin Moya Corral; D. Josué G. P. Espínola; Dr. Juliana Marchi; Dr. Juliana Marchi; Dr. Kai Jiang; Dr. Katia Cristiane Gandolpho Candioto; Dr. Kengo Imakuma; Dr. L. da Conceição; Dr. Lucas C. V. Rodrigues; Dr. Lucio Salgado; Dr. Luiz Antonio de Oliveira Nunes; Dr. Luiz Fernando Setz; Dr. Luiz Filipe C. P. de Lima; Dr. M. Kleitz; Dr. Magnus A. Gidlund; Dr. Marcelo Yoshimoto; Dr. Marcio R. Morelli; Dr. Márcio W. Mendes; Dr. Marco A. Guedes; Dr. Marco C. Bottino; Dr. Margarida J. Saeki; Dr. Maria Edileuza F. Brito; Dr. Maria Elena Leyva; Dr. Marja Malkamaki; Dr. Mika Lastusaari; Dr. Oscar M. L. Malta; Dr. Paulo Francisco Cesar; Dr. Pavel Novak; Dr. R. V. França; Dr. Renato Altobelli Antunes; Dr. Renato Baldan; Dr. Renato Hunter; Dr. Roberval Stefani; Dr. Rodrigo Moreno Botella; Dr. Rosa M. Rocha; Dr. Rubens Chiba; Dr. Rubens Nisie Tango; Dr. S. K. Tadokoro; Dr. Stela M. C. Fernandes; Dr. Sidney José Lima Ribeiro; Dr. Taneli Laamanen; Dr. Thomaz Augusto G. Restivo; Dr. Vagner Faustino; Dr. Vania H. Trombini; Dr. Waldemar A. Monteiro; Dr. Wilson Acchar; Dr. Xabier Turrillas; MSc. Lucas Hian da Silva; Álvaro A. Queiroz; Anderson Emanuel de Mello; Argemiro Soares da Silva Sobrinho; Bruno Geoffroy Schuraccio; Carla Costa Guimarães; Carlos Eduardo Podestá; Caruline S. C. Machado; Edílson Rosa Barbosa de Jesus; Edson Souza de Jesus Filho; Eliene Menezes; Eugênio T. Carvalho Filho; Fabiano Yokaichiya; Felipe de Oliveira; Felipe Gracio; Gonçalo Siqueira; Guilherme Wolf Lebrão; Hamilton Perez Soares Corrêa; José Carlos dos Santos; José Gabriel Vicente; Leandro César Pereira Gomes Safra; Lourival Bohes; Marcio Ferreira Hupallo; Marco Antônio Colosio; Marcos Gonzales Fernandes; Marcos Massi; Marcos Tadeu D'Azeredo Orlando; Mariana X. Milagre; Oswaldo P. V. Silva Júnior; Ranulfo Benedito de Paula Miranda; Ricardo Luiz Ciuccio; Ronaldo Câmara Cozza; Sérgio Allegrini Júnior; Sérgio Ciampolini de Lima; Sérgio Luís de Jesus; Tomaz Puga Leivas.

**Honor Mention and Awards**

In the Brasiltec and Viniltec Congress held in São Paulo (SP); 14-15 August; 2013; the SPE Brazil - Society of Plastics Engineers - gave the prize of best poster to the work “Preparation and characterization of a bio-composite prepared from high density polyethylene and husk fiber from brazilian chestnut” developed by R.D. Campos; M.S. Ferreira; F.R.V. Díaz; E.A.B. Moura and E.S.M. Seo.

In The VIII Meeting of Physics ITA held in São José dos Campos (SP); 08-12 June; 2013; the research “Study of the mean crystallite size and microstrain of ZnO using a non-ideal standard material” developed by R.U. Ichikawa; L.G. Martinez; K. Imakuma; X. Turrillas; M. Gusatti and H.G. Riella was awarded as the best master degree work.

The Brazilian Ceramic Society honored the work “Galvanic waste glasses: Do transition metals contribute to devitrification?” developed by A.C. da Silva; L.F. Setz; S.C. Santos and S.R.H. Mello Castanho as the second best work of the 57th Brazilian Congress on Ceramics held in Natal (RN); 19-22 May; 2013.

In the 19th Symposium on Electrochemical Methods in Corrosion Research held in Maragogi (AL); 18-23 November; 2012; the prize for best poster sponsored by ISE was awarded to W.I. Santos; J.M. Ferreira JR.; M. Oliveira; S.J. Hinder and I. Costa for the work “Corrosion protection of the clad on AA2024-T3 by cerium based conversion coatings”.

In the 56th Brazilian Congress on Ceramics held in Curitiba (PR); 03-06 June; 2012; the paper “Effect of the sintering temperature and time on phase assemblage and electrical conductivity of zirconia-scandia-ceria” developed by R.L. Grosso and E.N.S. Muccillo was awarded as the best work of the meeting.

The Brazilian Society of Automotive Engineering (AEA) during the 6th AEA premium 2012 - academic category - honored the work “DLC-coated cylinder liner for reducing fuel consumption” realized by E.D. Rejowski and M.F. Pillis.

In the MEV Summer School and ATR/NSUF User Week 2012 held in Idaho Falls - EUA; the prize to the best poster was awarded to the work “Evaluation of red mud-based glasses as nuclear wastform” developed by H. Vieira; R.K. Brow and J.R. Martinelli.

Best work of the Eighth International Latin American Conference on Powder Technology (PETCH 2011) held in Florianópolis (SC); 6-9 November; 2011; was awarded to the contribution titled "Evaluation of valve seat inserts for two categories of sintered materials” developed by R.A. Marques; D. Santos Filho; M.A. Colosio; M.A. Marques; J.C. dos Santos; L. Salgado; I.P. dos Santos and J.L. Rossi.

The Brazilian Ceramic Society honored the research “The effect of CTAB on synthesis in butanol of samaria and gadolinia doped ceria-nickel oxide ceramics” developed by A.R. Arakaki; S.M. Cunha; W.K. Yoshito; V. Ussui and D.R.R. Lazar as the best post-graduate work of the 55th Brazilian Congress on Ceramics held in Porto de Galinhas (PE); 29 May to 1st June; 2011. For the work “Use of spent catalyst of the Fluid Catalytic Cracking Units (FCCU) to produce glass frits” the researchers U.S. Prado; J.R. Martinelli; J.A.S. Souza and L.L. Silva were awarded as third best paper of the meeting.